Multiomics uncovers the epigenomic and transcriptomic response to viral and bacterial stimulation in turbot

Oscar Aramburu [1]*, Belén Gómez-Pardo[1], Paula Rodríguez-Villamayor[1], Andrés Blanco-Hortas[1], Jesús Lamas[1], Pooran Dewari[2], Diego Perojil-Morata[2], Pierre Boudinot[3], Daniel J. Macqueen[2], Carmen Bouza[1], Paulino Martínez[1*]

[1] University of Santiago de Compostela, Spain

[2] The Roslin Institute and Royal (Dick) School of Veterinary Studies, University of Edinburgh, Easter Bush Campus, UK

[3]Université Paris-Saclay, INRAE, UVSQ, VIM, Jouy-en-Josas, 78350, France.

* Corresponding authors

Abstract

Uncovering the epigenomic regulation of immune responses is essential for a comprehensive understanding of host defence mechanisms, though remains poorly investigated in farmed fish. We report the first annotation of the innate immune regulatory response in the turbot genome (Scophthalmus maximus), integrating RNA-Seq with ATAC-Seq and ChIP-Seq (H3K4me3, H3K27ac and H3K27me3) data from head kidney (in vivo) and primary leukocyte cultures (in vitro) 24 hours post-stimulation with viral (poly I:C) and bacterial (inactive *Vibrio anguillarum*) mimics. Among the 8,797 differentially expressed genes (DEGs), we observed enrichment of transcriptional activation pathways in response to Vibrio and immune pathways - including interferon stimulated genes - for poly I:C. We identified notable differences in chromatin accessibility (20,617 in vitro, 59,892 in vivo) and H3K4me3-bound regions (11,454 in vitro, 10,275 in vivo) between stimulations and controls. Overlap of DEGs with promoters showing differential accessibility or histone mark binding revealed significant coupling of the transcriptome and chromatin state. DEGs with activation marks in their promoters were enriched for similar functions to the global DEG set, but not always, suggesting key regulatory genes being in poised state. Active promoters and putative enhancers were enriched in specific transcription factor binding motifs, many common to viral and bacterial responses. Finally, an in-depth analysis of immune response changes in chromatin state surrounding key DEGs encoding transcription factors was performed. This multi-omics investigation provides an improved understanding of the epigenomic basis for the turbot immune responses and provides novel functional genomic information, leverageable for disease resistance selective breeding.

Keywords: turbot, immune response, epigenomics, chromatin state, transcription factor.

INTRODUCTION

The functional annotation of farm animal genomes is important for understanding traits with complex genetic architecture, such as disease resistance, growth, feed efficiency or reproduction (Andersson et al., 2015; Tuggle et al., 2016; Giuffra et al., 2019; Clark et al., 2020). Until recently, functional annotation mainly focused on protein-coding genes using transcriptomics. Transcriptome annotation is now consolidated with robust pipelines (Raghavan et al., 2022) and, throughout the years, transcriptome annotations for human (Frankish et al., 2023), model species (He et al., 2020; Lawson et al., 2020), terrestrial livestock (Summers et al., 2020; Halstead et al., 2021; Overbey et al., 2021) and some aquaculture species (Ramberg et al., 2021; Johnston et al., 2024) have been published.

Non-coding regulatory elements, including promoters, enhancers, silencers and insulators, have been studied in several livestock species but are mostly unexplored in aquaculture species. These elements play essential roles in regulating gene expression and their state can change depending on tissue, cell type, sex, age, and health status (Kellis et al., 2014). Thus, annotation of regulatory elements in different contexts not only aids to address basic questions related to morphology and physiology (Halstead et al., 2020; Pan et al., 2023), but also functional genomic responses to environmental variation (Feinberg, 2007; Ecker et al., 2018; Hu and Barrett, 2017). Genetic variation at non-coding elements also underpins phenotypic variation (Villar et al., 2020; Boltsis et al., 2021), and can thus be leveraged to improve our ability to predict polygenic traits using genomic data (Zhu et al., 2023). In this respect, more than 90% of phenotype-associated single nucleotide polymorphisms (SNPs) identified in human genome-wide association studies (GWAS) are located in non-coding regions (Giral et al., 2018), with similar results reported for livestock (Prowse-Wilkins et al., 2021).

In the past decade, human and livestock functional annotation initiatives have investigated epigenetic mechanisms involved in gene regulation through the study of chromatin state modifications across the genome (Yan et al., 2020a). Chromatin can switch dynamically between active and inactive states in minutes to hours, leaving epigenetic footprints that can be transmitted vertically following DNA replication (Moazed, 2011; Cuvier and Fierz, 2017). Many different sequencing assays have been developed to infer chromatin epigenetic status, including chromatin accessibility (ATAC-Seq; Buenrostro et al., 2015), protein-DNA interactions (ChIP-Seq; Park, 2009) and long-range chromatin interactions (Hi-C; van Berkum et al., 2010). These and other assays are being applied by the FAANG Consortium (Functional Annotation of Animal Genomes; Fang et al., 2019; Foissac et al., 2019; Liu et al., 2020; Clark et al., 2020). Current annotations of chromatin state and regulatory elements remain limited to a few terrestrial farm animal species (Summers et al., 2020, Pan et al., 2021; 2023; Xiang et al., 2021). However, a catalogue of regulatory elements is being generated for several important fish species used in global aquaculture (Johnston et al., 2024), currently the fastest growing animal production sector (Subasinghe et al., 2009; Troell et al., 2023).

Turbot (*Scophthalmus maximus*) is a valuable farmed fish in Europe and Asia (more than 100,000 tons), with the highest production in China (Gao et al., 2023) followed by Spain (APROMAR 2022). Turbot is in its 6th generation of selective breeding and infectious disease outbreaks constitute one of the main challenges this young industry faces (Martínez et al., 2021; Gao et al., 2023). This is a broader trend shared by global aquaculture, where infectious diseases cause losses of totalling more than 5,000 M€ per year (Mishra et al., 2018). Functional annotation of the turbot transcriptome has been performed against high-quality reference genomes (Figueras et al., 2016; Maroso et al., 2018; Xu et al., 2020; Martinez et al., 2021), including for immune-

organs stimulated with viruses (Diaz-Rosales et al., 2012), bacteria (Millán et al., 2011; Libran-Pérez et al., 2022) and parasites (Pardo et al., 2012; Robledo et al., 2014; Ronza et al., 2016; Valle et al., 2020). Candidate genes for disease resistance have been further explored by mapping differentially expressed genes (DEGs) within QTL regions (Martínez, 2016; Saura et al., 2019; Aramburu et al., 2023). However, limited attention has been given to non-coding regulatory elements, beyond a recent analysis of chromatin accessibility focussed on early development (Guerrero-Peña et al., 2023). How chromatin state and non-coding regulatory elements are regulated during immune responses remains undefined in turbot and scarcely explored in other farmed finfish.

The head kidney has been targeted in all previous functional genomics studies in turbot investigating pathogen responses (Millán et al., 2011; Díaz-Rosales et al., 2012; Pardo et al., 2012; Robledo et al., 2014; Ronza et al., 2016; Librán-Pérez et al., 2022; Aramburu et al., 2023), due to its central role in fish immunity (Mokhtar et al., 2023). Head kidney is a key lymphoid organ in most marine fishes and, analogous to the mammalian bone marrow, responsible for the production of high leukocyte diversity, including B-lymphocytes, early-stage T-lymphocytes, as well myeloid cells such as granulocytes and monocytes/macrophages (Klosterhoff et al., 2015; Geven et al., 2017; Chen et al., 2022). Innate immunity provides the first line of defence against pathogens and acts following the binding of pathogen-associated molecular patterns (PAMPs) to germline pattern recognition receptors (PRRs), leading to various effector cellular functions targeting pathogen destruction and clearance.

The aim of this study was to generate the first comprehensive functional annotation of the innate immune response of turbot using a chromosome-level reference genome sequence (Martínez et al., 2021). Live fish and primary immune cell cultures were stimulated using mimics of viral and bacterial infections and compared to controls to capture changes in the transcriptome alongside chromatin accessibility and epigenetic state by integrating RNA-Seq, ATAC-Seq and ChIP-Seq data. The experimental design and assays followed the protocols established in the the European Commission Horizon 2020 AQUA-FAANG project (Grant Agreement 817923). We aimed to generate comparable datasets in response to the same bacterial and viral mimics in six commercially important farmed fish species: European seabass (*Dicentrarchus labrax*), gilthead seabream (*Sparus aurata*), rainbow trout (*Oncorhynchus mykiss*), Atlantic salmon (*Salmo salar*), common carp (*Cyprinus carpio*) and turbot (*Scophthalmus maximus*). Our results provide a deeper understanding of the epigenomic basis for innate immunity in turbot and a novel resource to prioritize genetic variation associated with non-coding elements regulating immune responses.

RESULTS

Raw sequencing data and sample metadata

A total of 186 multiomic datasets were produced in this study, including RNA-Seq (36), ATAC-Seq (36) and ChIP-Seq (108; 36 per histone mark, plus 6 ChIP-Seq input controls). Full information on samples and metadata is shared in Supplementary tables 1 and 2.

RNA-Seq

On average, 69,580,246 raw reads per library were produced across the 36 RNA-Seq samples, with 97.2 % mapping to the turbot genome (Supplementary table 3A). Principal Component Analysis (PCA) showed that 77 % of the transcriptome variance was explained by PC1, separating the *in vivo* and *in vitro* stimulations (Figure 1A). Despite all three *in vivo* conditions grouping

together, a suggestive spatial segregation was observed mainly across PC1, with the control at one end and the *Vibrio* stimulation at the other. For the *in vitro* stimulations, PC2 clearly separated the *Vibrio* stimulation from poly I:C and control samples, the last two showing some overlap (Figure 1B).

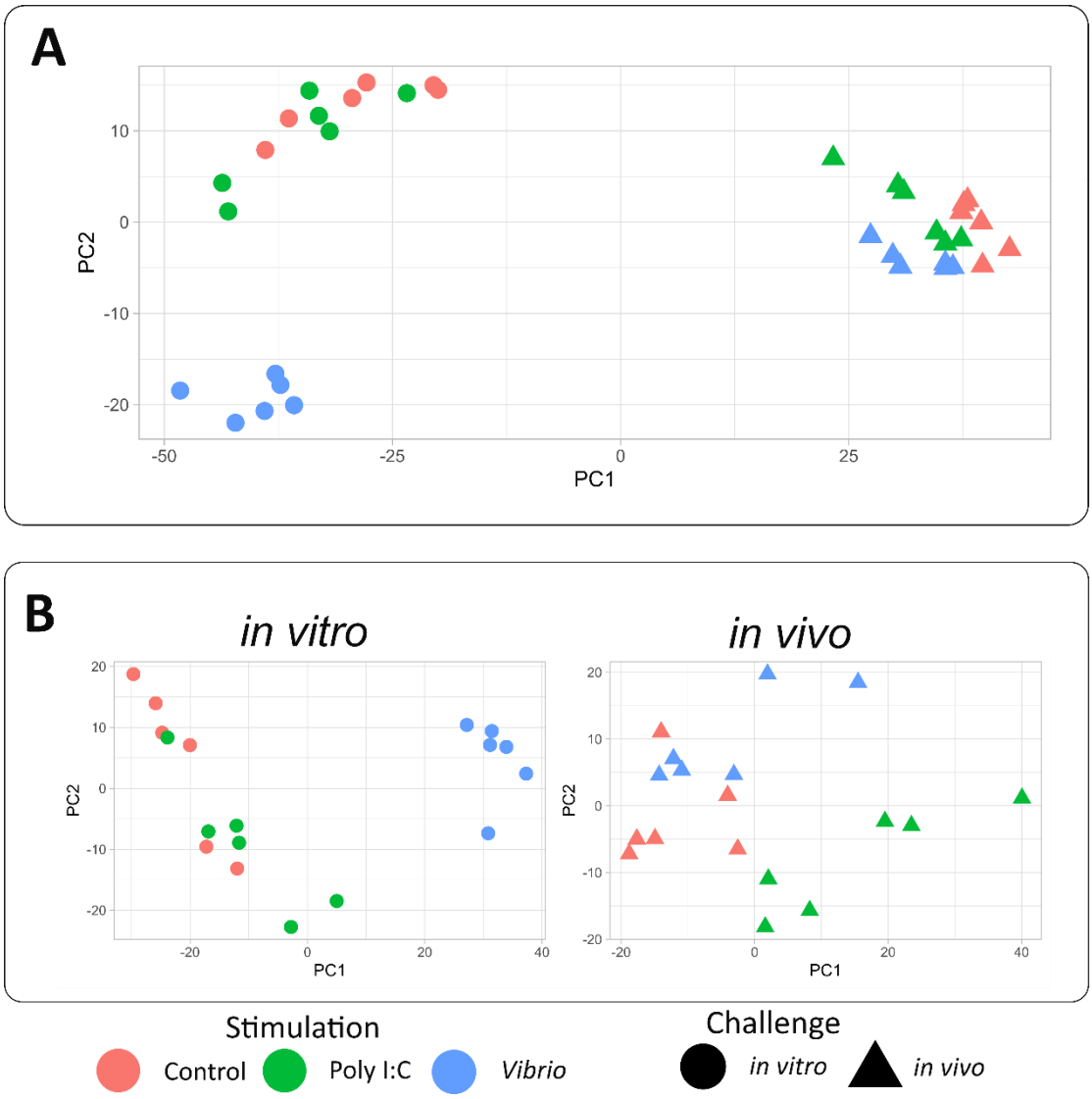

Figure 1. PCA of the *in vivo* and *in vitro* transcriptomic response to stimulation with poly I:C and *Vibrio*. **A)** PCA of the whole transcriptomic dataset; **B)** Independent PCAs for the *in vitro* and *in vivo* transcriptomic assays.

Differential expression analysis was performed by comparing each stimulated condition to the respective controls, both for the *in vitro* and *in vivo* stimulations. In total, 8,797 DEGs were identified across all comparisons (Table 1, Supplementary table 4). For the *in vitro* stimulations, a stronger response was observed for *Vibrio* than poly I:C stimulation, both for up and downregulated genes. Meanwhile, poly I:C showed a higher number of DEGs than *Vibrio* for the *in vivo* stimulations both for up and downregulated genes (Table 1, Supplementary table 4). Overall, more DEGs were detected in the *in vitro* than in the *in vivo* stimulations (7,940 vs 5,758, respectively).

119 **Table 1.** Number of differentially expressed genes (DEGs) for the *in vitro* and *in vivo* stimulations
120 with *Vibrio* and poly I:C

Stimulant	Stimulation	Downregulated DEGs	Upregulated DEGs	Total DEGs
Vibrio	*in vitro*	3,217	3,321	6,538
	in vivo	929	910	1,839
poly I:C	*in vitro*	544	858	1,402
	in vivo	1,918	2,001	3,919

121

122 **Functional enrichment among DEGs**

123 Gene Ontology (GO) analysis identified enriched biological processes for up and downregulated
124 DEGs in all conditions (Supplementary table 5). Among the downregulated DEGs, metabolism,
125 cell cycle and cytoskeleton organization terms were enriched for the *in vitro* stimulations, while
126 a limited number of terms were detected for *in vivo* stimulations (Supplementary table 5).

127 More abundant and specific enriched GO terms were detected among the upregulated DEGs.
128 Although RNA metabolism was enriched for most stimulations, poly I:C stimulation was linked to
129 a more specific activation of key immune functions (particularly *in vitro*) such as interferon-
130 stimulated genes and cytokine pathways, and regulation of toll-like receptors, besides more
131 general immune terms. DEGs for the *Vibrio in vitro* stimulation were enriched for immune-
132 related terms associated with cytokine and several transport pathways, whereas *Vibrio in vivo*
133 upregulated genes displayed strong enrichment of terms related to cytoskeleton organization,
134 tissue development and syncytium formation (Supplementary table 5).

135 Comparing upregulated DEGs between conditions, important immune-related GO terms were
136 commonly enriched between both poly I:C and *Vibrio in vitro* stimulations (Figure 2;
137 Supplementary table 6), including interferon type I stimulated genes (*socs1a, socs1b, nod2, nmi*),
138 cytokine signalling (the same genes plus *traf2*, *stat4* and *il15ra*) and major histocompatibility
139 complex type I (MHC-I) pathways (*erap1b*, *tapbpl*, *tapbp*.2). Activation of transcription, protein
140 localization, and a small number of terms associated with the immune-related "peptidyl-arginine
141 modification" (*prmt1, prmt3, prmt5, prmt7*) were commonly overrepresented in poly I:C and
142 *Vibrio in vivo*.

143 We detected several DEGs regulated in opposite directions for poly I:C and Vibrio stimulations
144 (Table 2; Figure 2; Supplementary table 6), suggestive of divergent immune response to bacteria
145 and virus. Among the *in vivo* upregulated DEGs for *Vibrio* and downregulated for poly I:C, we
146 observed enrichment of general immune functions, including genes such as *il-1b*, *traf4a* and *f2r*.
147 Conversely, immune-related genes including *nod2*, *sting1*, *irf1b* and *apaf1*, were downregulated
148 for *Vibrio* and upregulated for poly I:C *in vivo*. Interestingly, most genes involved in the type-I IFN
149 response orthologs of human and mouse (interferome database; Rusinova et al., 2023; Clark et
150 al., 2023) were upregulated in the poly I:C stimulations, while downregulated with *Vibrio*
151 extracts, especially in the *in vivo* stimulation (Table 2).

152 Considering condition-specific DEGs (Figure 2; Supplementary table 6), those upregulated by
153 poly I:C *in vitro* were enriched for terms associated with toll-like receptor signalling pathway
154 (*usp4, tasl, irak3*), while transcriptional activation terms were found among upregulated DEGs
155 for *Vibrio in vitro.* For the *in vivo* stimulations, transcriptional activation GO terms were enriched
156 for upregulated DEGs after poly I:C stimulation, whereas response to stimulus (explained by *tlr3,*

hamp, tnip1, fxc1a and *ccr12a*, among other genes) and syncytium formation (explained by *kirrel3l*, *jam2a*, *plekho1b*) were enriched for *Vibrio*.

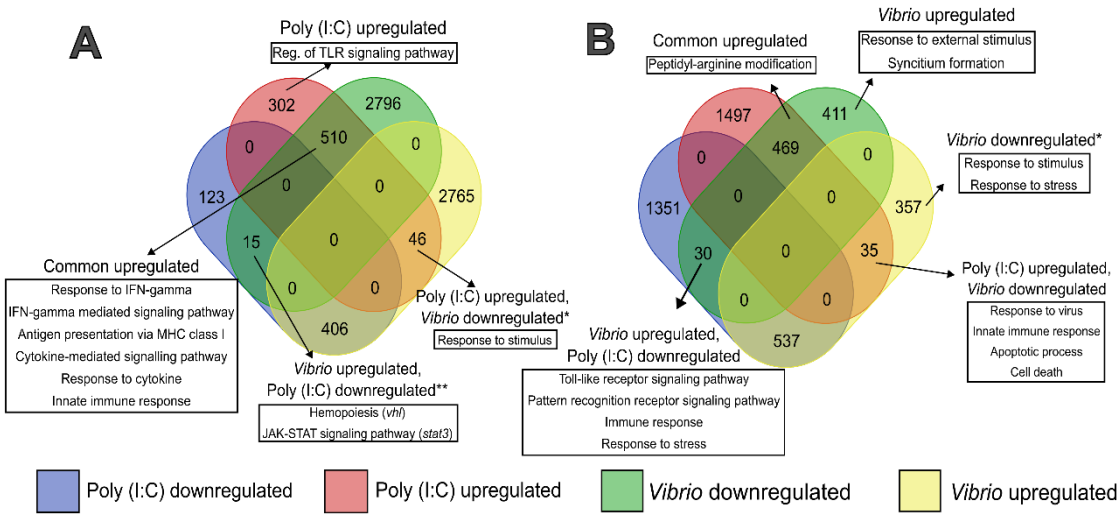

Figure 2. Venn diagrams illustrating overlap of DEGs for: **A)** *in vitro* poly I:C vs *Vibrio*, and **B)** *in vivo* poly I:C vs *Vibrio*. The white boxes show enriched GO terms related to the immune system found in specific subsets. Asterisks (*) highlight cases where suggestive immune-related GO terms were identified, despite not being significantly enriched. Double asterisks (**) highlight specific genes (in parentheses) associated with relevant immune functions. GO terms for the genes in the list were extracted from Ensembl-BioMart.

Table 2. Immune-related DEGs showing opposite responses following *Vibrio* and poly I:C stimulations.

Comparison	Differentially expressed genes (DEGs)
In vitro - upregulated by poly I:C, downregulated by *Vibrio*	***aldh2-like***, ***arhgap22***, *arrdc2*, *asb9-like* ***ascc3***, ***atxn7l1***, *bpifcl, c1qa,* ***cep170b***, *chaf1b, cnnm4b,* ***dync1h1***, ***ece2b***, ***ermp1-like***, ***gna14***, ***gpr155a***, ***has1***, ***ip6k2-like***, ***mapk8a***, ***mycbp2***, *nfkb1,* ***notch2***, *pld4-like, psda, rilp, serinc1-like, sgk2b, sp100.1,* ***spsb4a***, ***sptbn1***, *stim2b, synpr,* ***tank***, *tent4b,* ***tlr8***, *tmem269-like, tnk2b, tpm4b,* ***trim25-like***, ***trim35-14***, ***usp1***, *vcanb*
In vitro - upregulated by *Vibrio*, downregulated by poly I:C	*bcat-like, ctns, gid8b-like, pcxb,* ***psat1***, *rab11b-like, rtf2, sfxn2,* ***slc25a43***, ***stat3***, *thoc7, tollip, vhl, vps26c, vps41*
In vivo - upregulated by poly I:C, downregulated by *Vibrio*	*adora4a,* ***ankrd10b***, ***apaf1***, *arhgap12b, atg9a,* ***atxn7l1***, *bpifcl, camkk1b,* ***casp1a-like***, *cylda, emilin1,* ***fem1c***, *gfral,* ***gna14***, *gnptab, il22ra2,* ***irf1b***, *nlrc3-like,* ***nod2***, *nsmce4a, otulina,* ***parp15-like***, ***pstpip1b***, ***pstpip2***, ***rasgef1b***, *rnf146,* ***rnf170***, ***sting1***, ***themis2***, ***txk***, *ubp15, ucp2-like,* ***xcr1-like***, ***xkr8-like***
In vivo - upregulated by *Vibrio*, downregulated by poly I:C	*aebp1, alpl, anxa13l, anxa1a, cald1a, capn2b, chchd6a, col17a1-like, f2r, ggh-like, icn-like, il-1b, il8-like, il11-like, kdm2aa, lims2, map1lc3b, mfsd10, msto1, olfm5-like, osbpl10, plpp1like, plxnb2b, slc4a4-like, tlr13-like, traf4a, vat1, zan-like*

Turbot orthologs of human/mouse type I IFN stimulated genes (ISG) are highlighted (in bold upregulated and underlined downregulated), based on the database Interferome (Rusinova et al., 2013) and Clark et al. (2023). Note that most of these genes are downregulated in response to Vibrio anguillarum.

ATAC-Seq and ChIP-Seq

Excluding some ATAC-Seq *in vitro* libraries not associated with the type of stimulant, most libraries showed > 95% read mapping to the turbot genome (Supplementary table 3B). On average, we identified 24,251 (*in vitro*) and 62,013 (*in vivo*) peaks per sample for ATAC-Seq; 26,199 (H3K4me3), 13,461 (H3K27ac) and 27,765 (H3K27me3) peaks for the *in vivo* ChIP-Seq data; and 15,870 (H3K4me3), 5,363 (H3K27ac) and 38,784 (H3K27me3) peaks for the *in vitro* ChIP-Seq data. Samples in the PCA plot were mostly segregated across PC1, although PC2 explained most of the variance between histone marks, particularly differentiating repressive (H3K27me3) from active (H3K4me3 and H3K27ac) marks (Figure 3, Supplementary figure 1). *Vibrio* showed the greatest differentiation among the stimulations, while poly I:C and controls were mostly intermingled, particularly for ATAC-Seq (*in vitro* and *in vivo*) and H3K4me3-ChIP-Seq (*in vitro*).

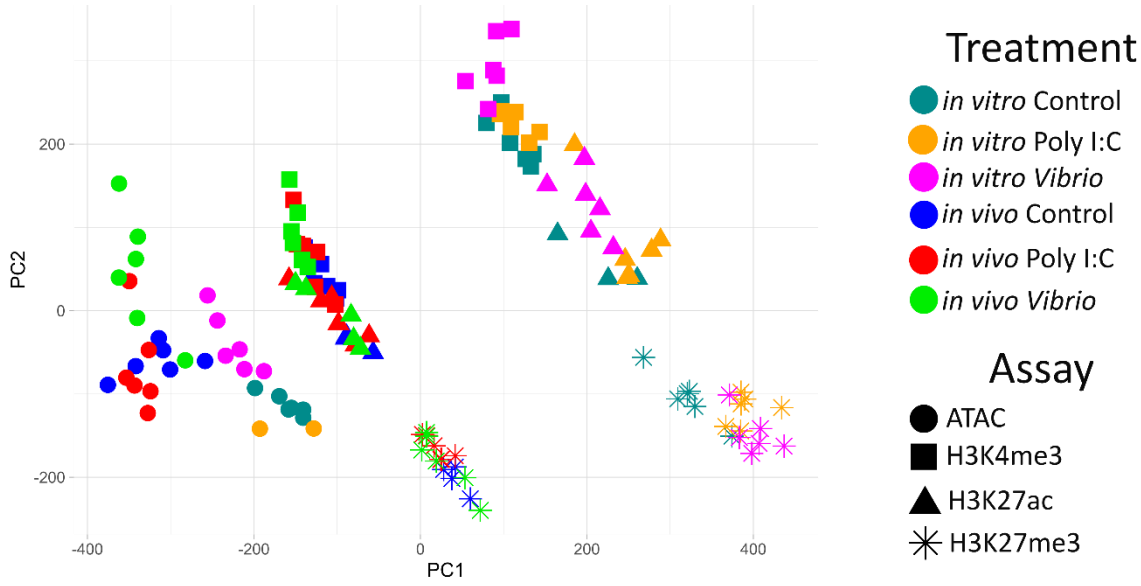

Figure 3. PCA of the *in vivo and in vitro* epigenomic response to stimulation with poly I:C and *Vibrio* for the open chromatin ATAC-Seq and histone ChIP-Seq (H3K4me3, H3K27ac, H3K27me3) samples.

ChIP-Seq blacklist

Certain genomic regions obscure epigenetic analyses because of anomalous, unstructured, or high signal due to particular genomic features (Amemiya et al., 2019). Using the 21 ChIP-Seq and µChIPmentation input controls (ENA project PRJEB57784) we constructed a blacklist of low confident genomic regions for turbot ChIP assays (Supplementary table 7). On average, 6.98 % (~39Mb) of the turbot genome was included in the blacklist, consisted of high input signal (5.58 %) and low mappability (1.40 %) regions (Supplementary figure 2).

Chromatin state annotation

Genome-wide chromatin state predictions were produced using ChromHMM employing the ChIP-Seq and ATAC-Seq data from stimulated and control samples from head kidney and leukocytes (Figure 4, Supplementary table 8). For the *in vivo* head kidney samples (Figure 4A), a 10-state model was chosen including promoters/transcription start sites (TSS; States 1, 2, 3 and 4), potential enhancer regions (States 5 and 6), ATAC islands (State 7, i.e. ATAC-peaks lacking histone marks), repressed regions (States 8 and 9) and low signal regions (State 10). For the *in vivo* leukocytes (Figure 4B), an 8-state chromatin model was chosen including promoters/TSS (States 1, 2 and 3), potential enhancer regions (States 4 and 5), ATAC islands (State 6), repressed regions (State 7) and low signal regions (State 8). For each chromatin state map, ±2kb regions around the TSS showed signal specifically for chromatin states 1, 2, 3 and 4 for head kidney (*in vivo*) and states 1, 2 and 3 for leukocytes (*in vitro*), mostly corresponding to promoter regions and/or transcriptionally active regions.

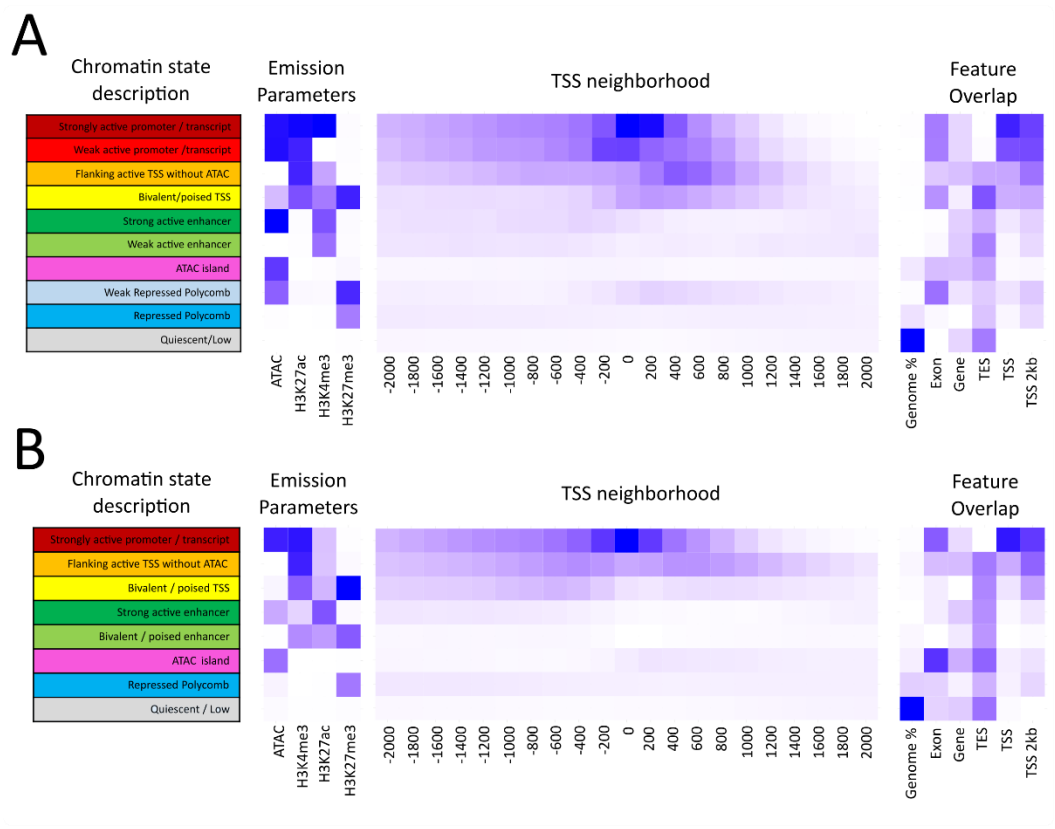

Figure 4. Chromatin state models of the turbot genome: **A)** 10-state model based on *in vivo* samples; **B)** 8-state model based on *in vitro* samples. Heatmaps of the emission parameters for each chromatin state are shown for ChIP-Seq data with three histone marks and ATAC-Seq (left), the neighbourhood around the TSS (middle) and the emission parameters of each chromatin state considered alongside features within the turbot genome (right). TSS: Transcription start site; TES: Transcription end site.

Differential chromatin accessibility regions (DAR) and differential histone modification regions (DHMR) following stimulation

We next aimed to identify regulatory regions in the turbot genome affected by the immune stimulation. Significant DARs and DHMRs (FDR-adjusted $p < 0.05$) comparing *Vibrio* and poly I:C stimulations to control samples were identified (Table 3, Supplementary table 9). Globally, a higher number of DARs or DHMRs were detected for up- than for down-regulated regions, more *in vivo* than *in vitro*, and more for *Vibrio* than poly I:C comparisons. Additionally, histone marks H3K27ac and H3K27me3 showed much lower DHMRs than H3K3me3 or ATAC-Seq DARs.

240 **Table 3.** Differential Accessibility Regions (DARs) and Differential Histone Modification Regions
241 (DHMRs) for the *in vitro* and *in vivo* immune stimulations with viral and bacterial PAMPs

PAMP	Stimulation	Assay	Downregulated DAR/DHMR	Upregulated DAR/DHMR	All DAR/DHMR
Vibrio	*in vitro*	ATAC	2,739	17,878	20,617
		H3K4me3	699	10,755	11,454
		H3K27ac	2	623	625
		H3K27me3	6	1,211	1,217
	in vivo	ATAC	43,159	16,733	59,892
		H3K4me3	287	9,988	10,275
		H3K27ac	0	3	3
		H3K27me3	4	0	4
poly I:C	*in vitro*	ATAC	0	0	0
		H3K4me3	0	0	0
		H3K27ac	0	20	20
		H3K27me3	0	0	0
	in vivo	ATAC	25	15	40
		H3K4me3	0	1,036	1,036
		H3K27ac	0	38	38
		H3K27me3	126	0	126

242

243 **Association of ATAC-Seq and ChIP-Seq data with RNA-Seq data**

244 We tested if DARs and DHMRs for H3K4me3 and H3K27ac marks annotated as promoter/TSS
245 regions (up to -1kb upstream of TSSs) corresponded to DEGs under the same experimental
246 conditions (Hypergeometric distribution test, $p < 0.05$). DARs and DHMRs were much more
247 overrepresented at the promoter regions of up- rather than down-regulated DEGs (Table 4,
248 Supplementary table 10), suggesting changes in chromatin state associated with the activation
249 of genes. We performed GO enrichment analyses of those upregulated DEGs within each
250 experimental condition t ($P < 0.05$, Table 4). Significant enrichment ($FDR < 0.05$) included several
251 metabolic activities and particular immune functions, including antigen processing/presentation
252 and apoptotic/cell death pathways (Supplementary table 11). Specifically, enriched terms were
253 mostly associated with RNA processing (in particular tRNA, rRNA, ncRNA), ribosome biogenesis,
254 and translation for the *Vibrio in vitro* stimulation, whereas for protein localization to nucleus and
255 organelle, DNA replication and carbohydrate metabolism for the *Vibrio in vivo* stimulation. The
256 term 'peptidyl-arginine modification' was also enriched involving *prmt1, prmt3, prmt5* and
257 *prmt7* genes, as outlined before for the whole DEG analysis (RNA-Seq). The poly I:C *in vivo*
258 stimulation showed enrichment in immune-related processes, including 'antigen processing and
259 presentation via MHC-I' (explained by *erap1b, tapbpl*) and 'regulation of programmed cell death'
260 (explained by *apaf1, bida, casp8 and 10, socs3a, grinab, bcl2l10*; Supplementary table 11).
261

262

263

264

265 **Table 4.** Overlap of promoter DARs and DHMRs with DEG promoters (Hypergeometric test, $p <$
266 0.05). Significant results are underlined. Refer to Supplementary table 10 for further details.

Experimental condition	DARs/DHMRs at promoter regions		Integration of DARs/DHMRs at promoter regions of DEGs			
			Down		Up	
	Down	Up	DEG	DAR/DHMR + DEG	DEG	DAR/DHMR + DEG
ATAC poly I:C *in vitro*	-	-	544	-	858	-
ATAC *Vibrio in vitro*	55	4922	3217	1	3321	1259
ATAC poly I:C *in vivo*	4	1	1918	0	2001	0
ATAC *Vibrio in vivo*	1350	6115	929	34	910	395
H3K4me3 poly I:C *in vitro*	-	-	544	0	858	0
H3K4me3 *Vibrio in vitro*	53	4289	3217	14	3321	1164
H3K4me3 poly I:C *in vivo*	-	368	1918	-	2001	151
H3K4me3 *Vibrio in vivo*	22	4024	929	3	910	242
H3K27ac poly I:C *in vitro*	-	0	544	-	858	0
H3K27ac *Vibrio in vitro*	0	72	3217	0	3321	49
H3K27ac poly I:C *in vivo*	-	4	1918	-	2001	3
H3K27ac *Vibrio in vivo*	-	1	929	-	910	1
Active prom poly I:C *in vitro*	-	-	544	-	858	-
Active prom *Vibrio in vitro*	106	6744	3217	15	3321	1782
Active prom poly I:C *in vivo*	4	370	1918	0	2001	151
Active prom *Vibrio in vivo*	1263	7082	929	37	910	463

267 *prom: promoter; DAR: differential accessibility regions; DHMR: differential histone modification*
268 *regions*

269 **Transcription factor binding motif (TFBM) analysis**

270 To establish TFs potentially associated with chromatin state regulation following immune
271 stimulation, the enrichment of TFBMs within DAR/DHMRs annotated as promoter or enhancer
272 regions were examined. Significant enrichment was detected for poly I:C *in vivo* and for *Vibrio in*
273 *vitro* and *in* vivo stimulations. On average across stimulations, 4 (range: 0-11) and 71 (range: 0-
274 132) enriched TFBMs were detected for down- and upregulated promoters, respectively, while
275 14 (range: 6-27) and 49 (range: 1-80) respective TFBMs were enriched for downregulated and
276 upregulated enhancers (Supplementary table 12).

277 Most TFBMs and associated TFs predicted for active promoters and enhancers were enriched in
278 several stimulations: 68 TFs for both *Vibrio* stimulations and *in vivo* poly I:C; 59 TFs for both *Vibrio*
279 stimulations; and 20 TF for both *in vivo* stimulations (Figure 5; Supplementary table 12).

280 To further investigate the functions of TFs with enriched motifs, we used the Molecular Complex
281 Detection algorithm (MCODE) and protein-protein interaction data (PPI) to identify connected
282 functions among differentially expressed TFs and among TFs with DARs or DHMRs on their
283 promoters (Supplementary figures 3 and 4, Supplementary table 13).

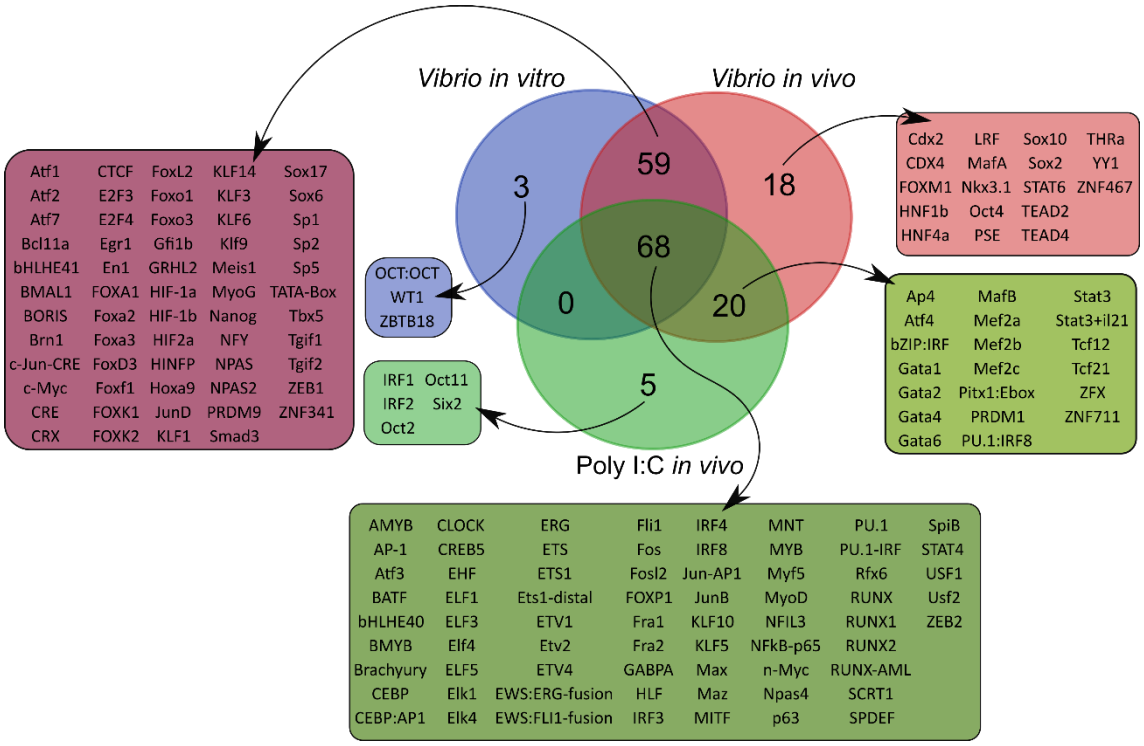

Figure 5. Venn diagram illustrating overlap of enriched transcription factor binding motifs (TFBMs) in upregulated promoter and enhancer regions in response to the different stimulants. Each coloured box shows the TFBM found.

For the *Vibrio in vitro* stimulation, interconnected clusters of TFs associated with hemopoiesis and immune functions, particularly myeloid leukocyte differentiation, FGF signalling pathway, regulation of neutrophil differentiation, lymphocyte activation, apoptosis and the ERK1/2 immune signalling, were identified. For the *Vibrio in vivo* stimulation, we detected clusters of TFs associated with similar functions (e.g. hemopoiesis, the ERK1/2 signalling pathway, myeloid cell development and cell death), but also other functions such as insulin signalling, regeneration, and oestrogen-dependent expression (Supplementary figures 3 and 4). Finally for the poly I:C *in vivo* stimulation, myeloid leukocyte differentiation, regulation of cell differentiation, cell morphogenesis and biosynthesis and growth showed connected TF subsets.

Using the Integrative Genomics Viewer (IGV), we visualized the variation in chromatin states around the promoters of 12 TF-DEGs selected from Supplementary table 13 to show the variance in chromatin state distribution across TFs and their regulatory elements following activation by the different stimulants (Figure 6; Supplementary Figure 5).

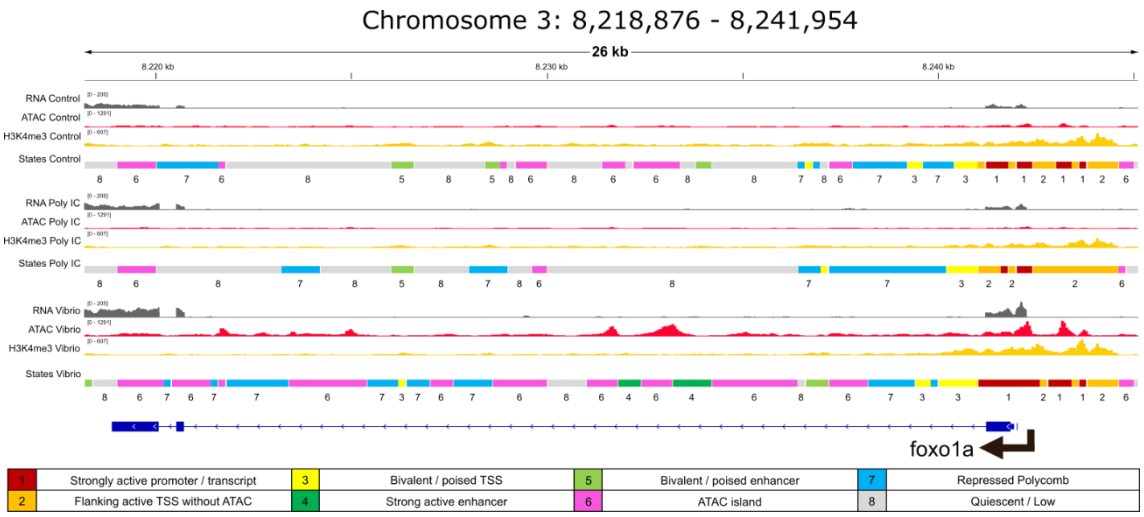

Figure 6. Chromatin state predictions and RNA/ATAC/ChIP-Seq tracks in the transcription factor coding gene *foxo1a*, which was upregulated and showed DAR around the promoter for *Vibrio in vitro* response. Transcription factor binding motifs for FOXO1A were also enriched in the promoter DARs of DEGs upregulated in response to *Vibrio in vitro.*

DISCUSSION

This study represents the first epigenomic analysis of the turbot head kidney, the primary hematopoietic and lymphoid organ of teleosts, in response to viral (poly I:C) and bacterial (inactivated *V. anguillarum*) mimics. While head kidney transcriptomic responses to bacteria, virus and parasites have been extensively investigated in turbot (Pardo et al., 2008; Millán et al., 2010; Domínguez et al., 2013; Díaz-Rosales et al., 2012; Robledo et al., 2014; Ronza et al., 2020; Valle et al., 2020; Libran-Pérez et al., 2022), the epigenetic regulation of chromatin states following immune stimulation has not been explored before. The head kidney response was explored through intraperitoneal injection, reflecting the response in the whole-body, including interactions among immune organs, and through *in vitro* stimulation of primary leukocyte cultures, reflecting their direct interaction with stimulants. The use of the same viral and bacterial mimics will enable further comparative evaluation among the six fish species included in the AQUA-FAANG project pertaining to five teleost orders (Salmoniformes, Cyprinidontiformes, Spariformes, Perciformes and Pleuronectiformes). We first discuss the transcriptional response to immune stimulations, which provide context to the chromatin assays performed to understand how transcription is regulated from transcription factors up to immune genes in the turbot.

Transcriptomic response to immune stimulation

Upregulated genes with key immune roles, such as interferon and cytokine pathways and toll-like receptor regulation, were found in both poly I:C stimulations and in *Vibrio in vitro* stimulation. Interferons (IFNs) are a subset of class II cytokines with crucial roles in immune response, especially against viruses but also intracellular bacteria (Gan et al., 2019). Interestingly, *tlr3*, encoding the toll-like receptor 3, which induces IFN production after interaction with poly I:C (Kumar et al., 2006), was upregulated in the *Vibrio in vivo* stimulation but not differentially expressed in poly I:C *in vivo* and downregulated after both *in vitro* stimulations. Signal exhaustion offers a plausible explanation for *tlr3* downregulation *in vitro*, with the 24-hour post-injection (hpi) sampling time missing the immediate interaction between leukocytes and stimulants. However, we cannot discard alternative hypotheses related to changes or diversification of the

336 TLR3 signalling pathway in flatfish or specifically in turbot, as suggested here by *tlr3* activation in
337 response to *Vibrio in vivo* stimulation and elsewhere to the parasite *P*. *dicentrarchi* (Figueras et
338 al., 2016). In fact, we identified other interferon-stimulated DEGs in poly I:C both *in vitro* and *in*
339 *vivo*, including *socs1a* and b (suppressor of cytokine signalling 1), *nod2* (nucleotide binding
340 oligomerization domain containing 2) and *nmi* (N-Myc interactor), typically participating in type
341 I IFN responses (Blumer et al., 2017; Ahn et al., 2021). *socs1* is an inducible negative regulator of
342 IFN (Blumer et al., 2017), a mechanism to maintain tissue homeostasis following the IFN
343 response; *nod2* encodes for an intracellular receptor triggering innate antibacterial and antiviral
344 signalling pathways, including IFN (Nie et al., 2017); and *nmi* increases STAT-mediated
345 transcription in response to IFN-gamma (Zhu et al., 1999). The activation of genes involved in
346 positive and negative regulation of IFN- signalling suggests a fine adjustment to an intense IFN
347 response to recover tissue homeostasis (Ivashkiv and Donlin, 2014; Murira and Lamarre, 2016).
348 Also, the upregulation of these four key genes after *Vibrio in vitro* stimulation is consistent with
349 past reports that place IFN regulation as a key point of the immune response (Kopitar-Jerala,
350 2017). In this regard, comparative analysis in the AQUAFAANG project will enlighten conserved
351 and specific mechanisms of immune response regulation across different farmed fish lineages.
352 Future studies in turbot should explore shorter periods following *in vitro* stimulation to provide
353 further understanding of the head kidney response to viral and bacterial mimics, as done in other
354 species (Hasanuzzaman et al., 2020; Herrera-Uribe et al., 2020).

355 Upregulated DEGs shared by both *in vivo* stimulations were involved in the activation of
356 transcription and translation and protein modification/localization. This included four members
357 of the immune-related protein arginine methyltransferase family (*prmt1*, *prmt3*, *prmt5* and
358 *prmt7*), enriched under the term "peptidyl-arginine modification". *prmt* family members
359 regulate transcription and translation and are also involved in signal transduction during
360 inflammation and response against poly I:C and bacterial lipopolysaccharide (LPS; Srour, 2022).
361 These four genes were also activated in both *Vibrio* stimulations, suggesting an important role in
362 the response to *Vibrio*.

363 We also verified if immune genes could be regulated in opposite directions after stimulation with
364 viral and bacterial mimics, which could reflect antagonistic immune responses. Increased
365 susceptibility to bacterial superinfections induced by innate antiviral responses has been
366 reported in several models in mammals (Barman and Metzger, 2021) in type I and type II IFN
367 responses (Navarini et al., 2006; Sun and Metzger, 2008). Such mechanisms are likely present in
368 teleosts due to the high conservation of these pathways, and in fact, different patterns of
369 resistance to viral and bacterial infections were observed among isogenic rainbow trout lines
370 (Fraslin et al., 2020). However, no negative correlations for resistance to bacteria and viruses has
371 been observed in the few studies addressing this issue in relation to selective breeding (Ødegård
372 et al., 2007; 2011; Bangera et al., 2011). Indeed, understanding the cellular basis of antagonistic
373 responses to viruses and bacteria in fish will require more research, but here we identified
374 examples of opposite gene expression responses, including genes from the core type I IFN
375 response, conserved between teleosts and humans (Levraud et al., 2019; Clark et al., 2023), such
376 as *sting1* (stimulator of interferon response CGAMP interactor 1, Zhang et al., 2021*), irf1b*
377 (interferon regulatory factor 1; Sullivan et al., 2021) and *nod2* (mentioned above),
378 downregulated by *Vibrio* and upregulated by poly I:C *in vivo*. Reciprocally, the critical pro-
379 inflammatory cytokine *il1b* (interleukin 1 beta, Sahoo et al., 2011) and the regulator of
380 inflammation *traf4a* (TNF receptor associated factor 4, Marinis et al., 2012) were upregulated by
381 *Vibrio* but downregulated by poly I: C. Interestingly, a majority of genes induced by poly I:C and
382 repressed by *Vibrio* extracts had human / mouse ISG orthologs (22/42 *in vitro*, 18/34 *in vivo*); in

383 contrast, many genes induced by *Vibrio* extracts and repressed by poly I:C, especially *in vivo,* had
384 human/mouse orthologs downregulated by type I IFN. Overall, these observations indicate that
385 a significant part of these contrasted responses is mediated by genes functionally conserved
386 between fish and mammals.

387 **Epigenetic assays and their association with transcriptomic response**

388 Activation and recruitment of transcription factor (TF) subsets is at the top of the specific
389 transcriptome cascade response (Alvarez et al., 2020; Weidemüller et al., 2021). In our study, the
390 exploration of promoters of differentially expressed TFs, also involving differential accessibility
391 regions (DARs) and differential histone modification regions (DHMRs), barely showed changes in
392 the chromatin state distribution between treatments (Supplementary Figure 5). This is the case
393 for instance of egr*1* (early growth response 1), which plays a key role in cell survival, proliferation
394 and cell death, and regulates the expression of *il1b* and *cxcl2* (CXC motif chemokine ligand 2).
395 The same was observed for *meis1* (myeloid ecotropic viral integration site homeobox 1), related
396 to bone marrow hematopoiesis in mammals, and *zeb2* (zinc finger e-box binding homeobox 2),
397 associated with macrophage infiltration (Taylor et al., 2022). In all these examples, the TF genes
398 showed bivalent/poised promoters in the three *in vivo* samples (control, *Vibrio* and poly I:C). A
399 similar situation was found *in vitro*, where promoters of genes, such as *irf3* (interferon regulatory
400 factor 3) and *mitf* (melanocyte inducing transcription factor), showed activation signals
401 regardless of the experimental condition. In previous studies, these bivalent/poised states have
402 been interpreted as a mechanism allowing rapid responses, e.g. for genes induced during the
403 pro-inflammatory response (Herrera-Uribe et al., 2020; Martínez de Paz and Josefowicz, 2021)
404 or during mammal embryonic development and in germ cells (Lesch and Page, 2014; Barbieri et
405 al., 2017). Thus, the expression of primary response genes, such as the TF genes exemplified
406 above, may be allowed by permissive chromatin states.

407 The presence of differential activation signals at promoter regions, either in the form of open
408 chromatin regions or the histone marks H3K4me3 and H3K27ac, are associated with differential
409 gene expression (Stępniak et al., 2021). H3K27ac is widely accepted as one of the most dynamic
410 activation marks in eukaryotes (Saeed et al., 2014). Interestingly, we did not find important
411 changes between experimental conditions in our study, where H3K4me3 was the most dynamic
412 among the ChIP-Seq marks. We suspect that the increase in H3K4me3 could also be an effect of
413 sampling being conducted 24 hours post inoculation (hpi)pi, especially for the *in vivo*
414 stimulations. Previous studies have reported that H3K4me3 may not have an active role in
415 activating transcription, an effect that should be detectable early after stimulation, but instead
416 in marking transcriptional activity itself, suggesting that H3K4me3 modification may have a role
417 in maintaining transcriptional consistency or memory of previous states (Howe et al., 2017).

418 DEG promoters overlapped with DAR/DHMRs for upregulated genes in most conditions (Table
419 4). GO enrichment of DEGs with activation signals at promoters (Supplementary table 11) was
420 similar to that observed with the whole DEG dataset (Supplementary table 5). *Vibrio* stimulations
421 were particularly enriched in terms associated with transcription activation, but also with some
422 immune functions, while poly I:C (especially *in vivo*) showed a more specific response, enriched
423 in immune-related processes (Supplementary table 6). However, DEGs associated with some key
424 immune functions in the transcriptomic analysis, such as response to cytokine stimulus, did not
425 show DAR/DHMRs, suggesting that these gene promoters could be already accessible before
426 stimulation. Cytokines are one of the core initiators of the inflammatory response (Secombes et

427 al., 2001), thus a bivalent state, ready for activation or inactivation of expression, might explain
428 this observation (Figure 5).

429 Regardless of predicted chromatin states around gene promoters, we observed an increased
430 expression of immune-related genes following poly I:C and Vibrio stimulation suggesting further
431 chromatin unpacking (Table 3), even if chromatin state is not strongly affected. In fact, many
432 differential regions were detected between stimulations, particularly DARs (i.e. ATAC-Seq) and
433 DHMRs (for H3K4me3) for *Vibrio*. In comparison, fewer DARs and DHMRs were detected for the
434 poly I:C stimulations. We interpret these observations as a return, both in vivo and in vitro, to
435 the native chromatin state after 24 hpi, which may suggest the initial response at this point is
436 exhausted, as suggested by the transcriptomic data.

437 Predicted TFBMs enriched within DARs/DHMRs in the promoters and enhancer-state regions
438 predicted by ChromHMM of upregulated DEGs, provided a more detailed picture of regulatory
439 elements changed by the immune stimulations (Figure 5, Supplementary table 12). Most of the
440 enriched TFBMs were shared between at least two treatments, which supports their general
441 regulatory function. Among those shared between most stimulations (excluding poly I:C *in vitro*),
442 we found several TFBMs of the ETS-family, which are involved in cell proliferation, apoptosis and
443 lymphocyte development (Watson et al., 2002). We also found TFBMs enrichment of PU.1, a
444 master TF for the myeloid lineage, that promotes chromatin accessibility, also identified in a
445 similar study in pig (Turkistany and DeKoter, 2011; Chen et al., 2020; Herrera-Uribe et al., 2020).
446 PU.1 is thought to promote binding of other TFs that were enriched in our study, including AP1.
447 This protein is activated by TLRs during the immune response (Shan et al., 2018) and regulates
448 gene expression in response to cytokines, stress, and bacterial and viral infections (Kim et al.,
449 2014), and notably the IFN regulatory factors (IRFs, particularly IRF3, IRF4 and IRF8). The IRFs are
450 key regulators of innate antiviral and antibacterial responses in vertebrates including fish (Clark
451 et al., 2021; Han et al., 2023). The observed ontology enrichment clustering of these TFs
452 reinforces the similarities between the conditions in our study (Supplementary figures 3 and 4).

453 To illustrate the functionality of our turbot epigenomic atlas, we explored the chromatin state
454 changes in a selection of 12 TF genes (Figure 6, Supplementary Figure 5). These genes were
455 differentially expressed and showed DARs/DHMRs in their promoters. Immune-responsive
456 chromatin state remodelling was found, for instance, for *irf8* (interferon regulatory factor 8) in
457 the *Vibrio in vitro* stimulation. Here, an extension of the "strongly active promoter" state around
458 the TSS region was visible compared to the non-stimulated and poly I:C stimulated samples,
459 alongside an overall expansion of the "strongly active transcript" and "ATAC island" states
460 downstream. IRF8 is a key regulator of the NF-κB signalling pathway during inflammation, along
461 with IRF3 (Yan et al., 2020b). Both *irf* genes were differentially expressed in poly I:C and *Vibrio in*
462 *vitro* stimulations (*irf8* also in poly I:C *in vivo*) and showed promoter DARs in *Vibrio* stimulations.
463 Interestingly, chromatin state changes were barely observed in the vicinity of the *irf3* promoter
464 (Supplementary Figure 5).

465 Another example was found in *Vibrio* and poly I:C *in vivo* stimulations for *bcl11a* (BCL11
466 transcription factor A), a key regulator of dendritic cell differentiation (Ippolito et al., 2014) and
467 negative regulator of p53 (Yu et al., 2012). This gene was differentially expressed in both
468 stimulations, but only showed a DAR promoter in response to *Vibrio* stimulation. The
469 promoter/TSS region was annotated by ChromHMM as "weak repressed Polycomb" in the
470 control, which changed in both the *Vibrio* and poly I:C stimulations, extending to
471 "bivalent/poised" state, and in the case of *Vibrio* showing an extension to "Strongly active

472 promoter/transcript" state. Weak and strong signals of active enhancers were also detected in
473 the poly I:C and *Vibrio* stimulations within the second intron of the *bcl11a*, that were not present
474 in the controls (Supplementary Figure 5). A similar situation was found *in vitro* for *foxo1a*
475 (Forkhead box O1), a TF-coding gene that participates in mucosal (innate) immune response
476 regulating the expression of antimicrobial peptides and promoting phagocytosis during bacterial
477 and parasitic infections (Cabrera-Ortega et al., 2017; Graves and Milovanova, 2019). This gene
478 was differentially expressed in *Vibrio in vitro* and showed an extension of the "Strongly active
479 promoter" state compared to the control and specially the poly I:C stimulation, while conserving
480 the "bivalent/poised TSS" stretches downstream of the promoter. This was followed by many
481 "ATAC islands" along the gene that were also present, although more scarcely, in the control, and
482 almost absent in poly I:C. Finally, a "medium enhancer" state was detected within the first intron,
483 present only in the *Vibrio* condition. These observations highlight the relevance of epigenetic
484 chromatin marks at the first intron and other intronic regions associated with gene expression
485 modulation (Jo and Choi 2019; Johnston et al. 2019), as target regulatory annotations to explore
486 functional variants for disease resistance and selective breeding.

487 **Conclusions and perspectives**

488 In summary, our study provides the first atlas of regulatory elements in turbot head kidney and
489 leukocytes during the early response to viral and bacterial stimulation, as a contribution to the
490 AQUA-FAANG project within the umbrella of the FAANG initiative. The integration of ATAC-Seq
491 and ChIP-Seq data suggests that changes in chromatin state distribution were not as frequent
492 between stimulations and controls as expected. However, the presence of DARs and DHMRs
493 between the stimulations and the controls, which broadly overlapped with DEGs, provides clear
494 evidence for gene regulation at the epigenetic level that underpins changes in gene expression
495 driving immune functions. Overall, this epigenomic atlas will help to decode the molecular
496 mechanisms underlying turbot immune responses to viral and bacterial stimuli and offers a novel
497 resource for developing selective breeding strategies for controlling diseases, one of the main
498 concerns of turbot industry. Future work will benefit from linking the regulatory annotations
499 generated in this study with genetic variants defined by whole genome re-sequencing (Johnston
500 et al., 2024), to help prioritize causal genetic variants for disease resistance traits underpinned
501 by gene expression responses to pathogens.

502 **METHODS**

503 **Animals**

504 Thirty 8-month-old immature turbot specimens provided by Stolt Sea Farm SA (Ribeira, Spain)
505 were housed in indoor tanks with recirculating seawater at the facilities of the Aquarium of the
506 University of Santiago de Compostela (Spain) for a period of acclimation of 15 d at 16 °C
507 (Supplementary table 1). All fish were fasted for 24 h before stimulations were performed.
508 Eighteen fish were stimulated *in vivo* by intraperitoneal injection, while the other 12 were used
509 for leukocyte isolation for *in vitro* stimulation (see following sections). Fish were anesthetized by
510 bath (MS-222; 100mg/L) and then euthanized by anaesthetic overdose (MS-222; 150 mg/L)
511 before tissue sampling. All animal procedures were approved by the Bioethics Committee of the
512 University of Santiago de Compostela (body authorized according to R.D. 53/2013) and with the
513 authorization of the Xunta de Galicia Regional Government.

514 **Protocols**

515 Detailed protocols for the *in vivo* and *in vitro* stimulations, RNA isolation, ATAC-Seq and ChIP-Seq
516 (including library preparation) followed for turbot are available in the FAANG repository
517 (data.faang.org; URLs for protocols in Supplementary tables 1 and 2).

518 ***In vivo* immunostimulation**

519 Six fish were used per experimental condition for the *in vivo* stimulations: i) poly I:C for viral
520 mimic immunostimulation; ii) killed *Vibrio anguillarum* for bacterial immunostimulation; and iii)
521 phosphate buffered saline (PBS) for control. For poly I:C (Sigma P1530), we prepared a working
522 stock at 5 mg/ml in PBS, preheated to 55 °C (15 min) and cooled at room temperature (20 min)
523 before use. Fish were then injected intraperitoneally with 5 µg per g fish weight. For bacterial
524 immunostimulation, an extract of *V. anguillarum* (strain P0382; INRA, France) was used. Bacteria
525 were cultured in a tryptic soy broth medium to an OD600 (optical density at 600 nm) of 1.5. The
526 bacterial pellet (derived from 100 ml of full-grown culture) was washed in an isotonic solution
527 of NaCl (9 g/L) four times and resuspended in 1 ml of the same solution. Bacteria were killed by
528 incubation for 30 sec at 100 °C, allowed to cool at room temperature and stored at -80 °C. The
529 bacteria extract was inoculated in each specimen, diluted in PBS (1:10) for a final volume of 100
530 µl. Control fish were injected with 100 µl of PBS. After 24 h, head kidney samples were extracted,
531 washed with PBS and cut into at least three pieces (> 20 mg each); two were flash frozen on dry
532 ice for ATAC-Seq and ChIP-Seq and the other was immersed in RNAlater (Thermofisher Scientific)
533 for RNA extraction and RNA-Seq. All samples were then stored at -80°C (Figure 7A;
534 Supplementary table 2).

535 ***In vitro* stimulation: leukocyte isolation and culture**

536 Leukocytes were isolated from 12 fish. The entire head kidney was aseptically isolated and placed
537 in a Petri dish with 40 ml of cell isolation media (500 ml of Leibovitz L-15 medium (L-15), 10 ml
538 FBS (2 %), 0.02 % EDTA). Samples were then cut into small pieces and passed through a 100 µm
539 nylon mesh with constant flow of cell isolation media. Leukocytes were separated by
540 centrifugation of 40 ml of the cell suspension gently layered in a 50 ml tube containing 51 %
541 Percoll (400 x g, 30 min, 4 °C, no brakes). The interface layer was collected by centrifugation (400
542 x g, 10 min, 4 °C) and washed three times with L-15 medium containing 0.1 FBS, keeping the
543 pelleted leukocytes (Figure 7B).

544 To ensure enough cells were available, samples were pooled by pairs after cell counting and cell
545 viability was evaluated by the trypan blue exclusion test, totalling 6 pools (each 18 x 10^6 cells;
546 Supplementary table 1). Then, each pool was divided into nine aliquots of 2 x 10^6 cells (in 2 ml)
547 that were dispensed into wells, for a total of 54 wells (6 pools x 9 aliquots): 18 stimulated with
548 20 µl of poly I:C solution; 18 with 20 µl of inactivated *V. anguillarum*; and the remaining 18 wells
549 used as controls (Figure 7B). All leukocyte cultures were incubated for 24 h at 16 °C. Cells were
550 then collected in 2 ml Eppendorf tubes and pelleted at 500 x g for 5 mins at room temperature.
551 Eighteen pellets were resuspended in RNAlater and stored at -80 °C for RNA-Seq, while the other
552 36 were flash frozen in dry ice and stored at -80 °C for ATAC-Seq and µChIPmentation,
553 respectively (Supplementary table 1).
554

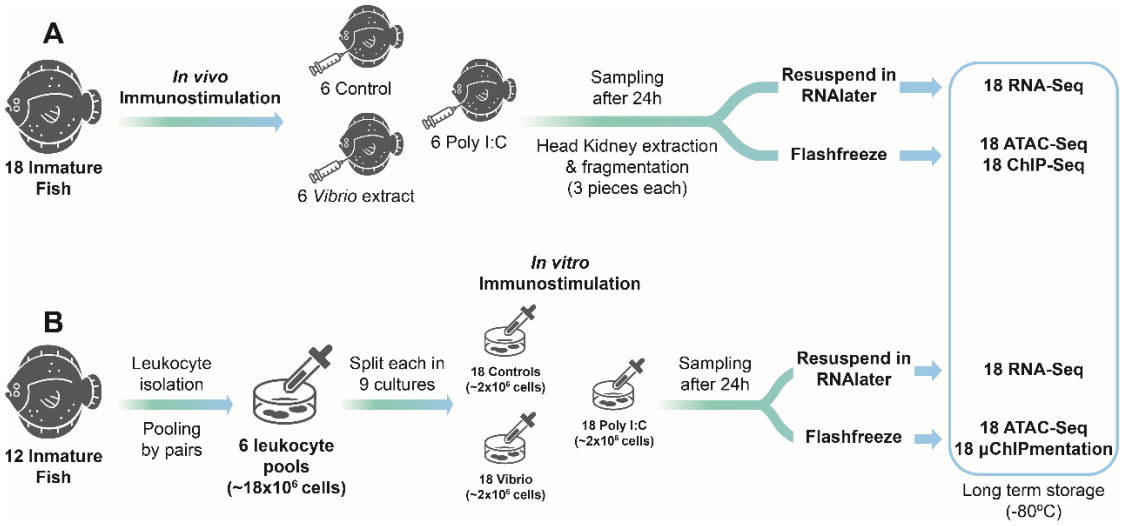

Figure 7. Experimental design followed for turbot immunostimulations: **A)** *in vivo* immunostimulation of immature fish with subsequent sampling of head kidney; **B)** *in vitro* stimulation of head kidney leukocytes of immature fish; 18 samples were used for RNA-Seq, 18 for ATAC-Seq and 18 for ChIP-Seq/µChIPmentation with antibodies to H3K4me3, H3K27ac and H3K27me3 histone marks.

RNA isolation and sequencing

After sample thawing, total RNA was extracted and purified using the miRNeasy Kit (QIAGEN) with specific modifications for: i) frozen head kidney (> 20 mg), following a protocol for "Total RNA extraction for tissues", and ii) frozen leukocytes (2 x 10^6 cells) following a protocol for "Total RNA extraction for frozen cells" (Supplementary table 2). RNA integrity and quantity were evaluated in a Bioanalyzer (Bonsai Technologies, Madrid, Spain) and in a NanoDrop® ND-1000 spectrophotometer (NanoDrop® Technologies Inc., Wilmington, DE, USA). RNA integrity number (RIN) averaged 8.3 across all samples, always above 7.3. RNA samples were delivered to Novogene (UK) for library preparation using NEBNext Ultra Directional RNA Library Prep Kits for Illumina and sequenced using an Illumina NovaSeq S4 platform to generate 150 bp paired end reads.

RNA-Seq data processing

RNA-Seq data was processed using nf-core/rnaseq 3.10.1 (Patel et al., 2023) run with default parameters, using the turbot Ensembl genome ASM1334776v1 (Martínez et al., 2021) as reference. In brief, the pipeline evaluated quality of raw reads using FASTQC (Andrews, 2010) and trimmed adapters and low-quality bases using Trim Galore! (Martin et al., 2011). Reads were then mapped using STAR (Dobin et al., 2013). Normalized transcript read counts were obtained using RSEM (Li and Dewey, 2011). After nf-core processing, the resulting count tables were filtered to remove genes with expression below 5 transcripts per million (TPM < 5) and represented in only one sample across all conditions.

Differential gene expression and gene ontology analysis

Differentially expressed genes (DEGs) between stimulated and control samples were identified using the R/Bioconductor package DESeq2 v1.38.1 (Love et al., 2014). Genes with false discovery rate (FDR) adjusted $p < 0.05$ were considered DEGs. Functional enrichment of the DEG lists was performed using ShinyGO v0.77 (Ge et al., 2020). Gene ontology (GO) terms for Biological

587 Process of each list were ranked by statistical significance (FDR-adjusted $p < 0.05$). All expressed
588 genes across conditions were used as the background for GO analyses.

589 **ATAC-Seq: Library preparation and sequencing**

590 Following a standard protocol for "Nuclei isolation for ATAC-Seq procedures" (Supplementary
591 table 2), the frozen head kidney fragments (> 20 mg; *in vivo* assay) and cell pellets ($2x10^6$ cells;
592 *in vitro* assay) were thawed and resuspended in 1 ml of TST buffer. Each tissue fragment was cut
593 into smaller pieces with a scalpel, mashed with the rubber back of a syringe, and filtered through
594 a 40 µm cell strainer, while cell pellets were resuspended by gentle pipetting. The number and
595 integrity of nuclei was assessed with a haemocytometer (minimum of ~50,000 nuclei in a 16.5
596 µl suspension; ~3,000 nuclei/µl) before carrying out the Tn5 transposase reaction with Illumina
597 Tagment DNA TDE1 enzyme (37°C, 30 min, 1000 RPM, Illumina) following the standard
598 "OmniATAC protocol" (Corces et al., 2017; Supplementary table 2). The resulting DNA was
599 purified with a MinElute PCR purification kit (Qiagen), and DNA concentration assessed with a
600 Qubit using the dsDNA HS kit (ThermoFisher Scientific). Library amplification (10-12 PCR cycles)
601 was carried out using the NEBNext Ultra II DNA Library Prep Kit (New England Biolabs), with IDT
602 for Illumina UD Indexes (96x, Plate A, Set 1, Illumina). Library size selection was performed to
603 remove fragments below 180 bp and above 700 bp using AMPure XP beads (Beckman coulter).
604 Finally, DNA fragment size distribution was assessed with the Bioanalyzer High Sensitivity DNA
605 Assay kit (Agilent Technologies). ATAC-Seq libraries were delivered to Novogene (UK) to be
606 sequenced on an Illumina NovaSeq S4 platform generating 150 bp paired end reads.

607 **ChIP-Seq and µChIPmentation: Library preparation and sequencing**

608 The frozen head kidney fragments (> 20 mg) and leukocyte pellets ($2x10^6$ cells) were thawed on
609 ice. Following a standard "ChIP-seq" protocol (Supplementary table 2), the tissue fragments were
610 transferred into a Douncer homogenizer containing a protease inhibitor cocktail (PIC, Roche, 1
611 tablet in 50 ml of PBS) solution immersed in ice and homogenized using pestles A and B (from
612 less to more plunger adjustment). The leukocyte pellets were resuspended in the PBS and PIC
613 solution. The amount and quality of nuclei was assessed with a haemocytometer and trypan
614 blue staining (> 10 million cells for head kidney; > 100,000 for leukocyte cultures). Due to the
615 low number of nuclei recovered from the leukocyte cultures, a µChIPmentation protocol
616 (Diagenode) was used, following a modified protocol (Supplementary table 2).

617 In both cases, chromatin crosslinking was done using a 1 % formaldehyde solution followed by
618 quenching with glycine (0.125 M). Nuclei were pelleted and resuspended in complete sonication
619 buffer, while leukocyte nuclei were resuspended in Hanks' Balanced Salt Solution (HBSS, Thermo
620 Fisher Scientific) - tL1 buffer (Supplementary table 2). The chromatin was sheared using a Covaris
621 S2 focused ultrasonicator with the following parameters: 2 % duty cycle, intensity 3, with 200
622 cycles per burst, at 4 °C for 8 min and 6 min for head kidney tissue and leukocytes, respectively.

623 The immunoprecipitation was performed using Diagenode antibodies for three marks: H3K4me3
624 (marking active promoter regions; cat. No. C15410003; 1.3 µg/µl), H3K27ac (marking active
625 enhancer and promoter regions; cat. No. C15410196; 2.8 µg/µl) and H3K27me3 (marking
626 Polycomb repressed regions; cat. No. C15410195; 1.1 µg/µl). For head kidney samples,
627 antibodies were coupled with pre-washed protein A and protein G beads, and the tubes left
628 under rotation overnight (~16 h) at 4 °C, following the standard ChIP-Seq protocol. After washing
629 the beads and decrosslinking, the samples were purified using the MinElute PCR purification kit
630 (Qiagen) and later quantified with DNA HS Qubit (ThermoFisher Scientific). Immunoprecipitated
631 chromatin was stored at -20 °C until library preparation, using a Microplex v3 kit (Diagenode).

632 For the leukocyte samples, the µChipmentation kit for histones (Diagenode) was used for
633 chromatin immunoprecipitation and ChIP-Seq library preparation (Supplementary table 2).

634 Before sequencing, the quantity and quality of purified libraries was assessed using the Qubit
635 DNA HS kit (ThermoFisher Scientific) and the High Sensitivity DNA Assay kit (Agilent
636 Technologies), respectively. A minimum of 60 % of the chromatin was required to have a size
637 distribution between 200-700 bp (centered around 350-400 bp). ChIP-Seq libraries were
638 delivered to Novogene (UK) for sequencing on an Illumina NovaSeq S4 platform generating 150
639 bp paired-end reads.

640 **ATAC-Seq and ChIP-Seq data processing**

641 ATAC-Seq and ChIP-Seq data were processed using the nf-core/atacseq v1.2.2. and nf-
642 core/chipseq v1.2.2 pipelines (Ewels et al., 2023), respectively, run with the narrow_peak option
643 for ATAC-Seq and H3K4me3 and H3K27ac ChIP-Seq datasets, and with the broad_peak option for
644 H3K27me3. The other parameters were kept by default. Quality assessment of the reads was
645 carried out with FASTQC (Andrews, 2010), and adapters and low-quality bases trimmed with Trim
646 Galore! (Martin et al., 2011). Reads were mapped to the turbot genome using BWA (Li and
647 Durbin, 2009). Further filtering was done with SAMtools (Danecek et al., 2021), BAMtools
648 (Barnett et al., 2011) and Pysam (Danecek et al., 2021). Genome-wide immunoprecipitation (IP)
649 enrichment relative to controls was done with deepTools (Ramírez et al., 2014) and
650 broad/narrow peaks were called using MACS2 (Zhang et al., 2008). Once nf-core was finished,
651 suboptimal replicates with very low peak numbers were excluded after visualizing their bigwig
652 files on the Integrative Genomics Viewer (IGV; Robinson et al., 2023).

653 **ChIP-Seq and µChIPmentation blacklist**

654 To improve the signal-to-noise ratio of the ChIP-Seq and µChIPmentation data, a blacklist
655 consisting of high signal and low mappability regions was constructed using ChIP-Seq and
656 µChIPmentation inputs, including 21 control ChIPseq turbot samples (ENA accession
657 PRJEB57784). The mappability of the turbot genome for read lengths of 100 bp and 150 bp (k-
658 mers 100 and 150) was quantified using the umap software package (Karimzadeh et al., 2018).
659 The generated mappability files were fed into the ENCODE blacklist software (Amemiya et al.,
660 2019) to generate the blacklist. Alignment and peak files derived from the nf-core pipeline were
661 filtered with BAMtools to remove reads and peaks located in the blacklist regions.

662 **Differential histone modification regions and differentially accessible regions**

663 Differential histone modification regions (DHMRs) and differentially accessible regions (DARs;
664 adjusted $p < 0.05$) between stimulated samples and controls were identified using DiffBind (Stark
665 and Brown, 2011) with default settings.

666 **Integration of ChIP-Seq and ATAC-Seq data with RNA-Seq data**

667 For each condition tested, the promoters of DEGs overlapping with regions tagged as DARs
668 and/or DHMRs were identified. When applicable, a hypergeometric test was performed to check
669 the significance of overlapping between each pair ($p < 0.05$).

670 **Chromatin state inferences**

671 Genome-wide chromatin states for each condition were predicted using ChromHMM (Ernst and
672 Kellis, 2012) integrating the ChIP-Seq data (µChIPmentation for *in vitro* samples) for the three
673 histone marks (H3K4me3, H3K27ac and H3K27me3) and ATAC-Seq data. Chromatin state

prediction was performed by testing ChromHMM models including from 8 to 15 states, keeping the one that returned the most biologically relevant chromatin states, for head kidney and leukocyte data separately (Pan et al., 2021; Baranasic et al., 2022; Vu and Enst, 2022). The genome-wide distribution of resulting chromatin states was visualized on IGV. Regions annotated as enhancer-related states by ChromHMM were retrieved, and each stimulation dataset was compared against its respective control to identify potential enhancer-related regions. Then, each list of regions including potential enhancers annotated as "intergenic" or "intron" were kept as differential enhancer-state regions for further analysis.

Transcription factor motif analysis

Enriched transcription factor (TF) binding motifs (TFBM) included in the HOMER software (Heinz et al., 2010) were identified using the *findMotifsGenome.pl* function (settings: -size given -mask -mset vertebrates) in the different lists of promoter-associated DHMRs/DARs and putative enhancers for each condition. Random genomic regions with GC-content matching each input genomic list were used as the background for automatic motif analysis by HOMER. Only TFBMs with $p < 0.01$ and percentage of target sequences > 5 % were considered enriched.

GO analysis of the TFs predicted to bind enriched TFBMs was performed with Metascape (Zhou et al., 2019) using zebrafish *Danio rerio* as the reference. Finally, a selection of TF genes that were DEGs and contained promoter regions overlapping DARs or DHMRs were explored with IGV (Robinson et al., 2023).

DATA ACCESS

All raw RNA-Seq, ATAC-Seq and ChIP-Seq datasets can be accessed through the ENA repository under accession numbers PRJEB47933, PRJEB47934 and PRJEB57784, respectively. Detailed metadata for the samples and prepared libraries are available in Supplementary tables 1 and 2, respectively. Detailed experimental protocols are publicly available in the FAANG repository (data.faang.org) and following the URLs facilitated in Supplementary tables 1 and 2.

COMPETING INTEREST STATEMENT

The authors declare no competing interests.

ACKNOWLEDGMENTS

We acknowledge the technical support and informatic resources provided by the Centro de Supercomputación de Galicia (CESGA). We acknowledge Professor Carolina Tafalla (INIA-CSIC) for the support given in the revision of this article.

AUTHOR CONTRIBUTIONS

OA: Methodology, Software, Formal analysis, Investigation, Data Curation, Visualization, Writing – original draft, Writing – review & editing; **BGP:** Methodology, Investigation, Resources, Writing – review & editing; **PRV:** Investigation, Resources, Writing – review & editing; **ABH:** Software, Formal Analysis, Data Curation, Visualization, Writing – review & editing; **JL**: Investigation, Resources, Writing – review & editing; **PD:** Software, Formal Analysis, Writing – review & editing; **DPM:** Software, Formal Analysis, Writing – review & editing; **PB**: Resources, Writing – review & editing; **DM**: Funding Acquisition, Methodology, Supervision, Resources, Writing – review & editing; **CB**: Conceptualization, Formal Analysis, Resources, Writing – review & editing, Project Administration, Supervision; **PM**: Conceptualization, Methodology, Formal Analysis, Resources, Writing – review & editing, Project Administration, Supervision.

FUNDING

This study was funded by the AQUA-FAANG project, which received funding from the European Union's Horizon 2020 research and innovation programme under grant agreement No 817923. Additional funding was provided by Xunta de Galicia local government (Spain) (ED431C 2022/33), which also supported the research fellowships of OA and PRV (refs. ED481A-2020/119 and ED481A-2020/491430, respectively). Contributions from the Roslin Institute were further supported by the BBSRC Institutional Strategic Programme grants BBS/E/D/10002070, BBS/E/D/20002174, BBS/E/RL/230001B and BBS/E/RL/230002B.

REFERENCES

Ahn JH, Park JY, Kim DY, Lee TS, Jung DH, Kim YJ, Lee YJ, Lee YJ, Seo IS, Song EJ et al. 2021. Type I Interferons Are Involved in the Intracellular Growth Control of *Mycobacterium abscessus* by Mediating NOD2-Induced Production of Nitric Oxide in Macrophages. Frontiers in Immunology, **12**. doi: 10.3389/fimmu.2021.738070.

Alvarez JM, Schinke AL, Brooks MD, Pasquino A, Leonelli L, Varala K, Safi A, Krouk G, Krapp A, Coruzzi GM. 2020. Transient genome-wide interactions of the master transcription factor NLP7 initiate a rapid nitrogen-response cascade. *Nature Communications*, **11**(1), 1157. doi: 10.1038/s41467-020-14979-6.

Amemiya HM, Kundaje A, Boyle AP. 2019. The ENCODE Blacklist: Identification of Problematic Regions of the Genome. *Sci Rep* **9**, 9354. doi: 10.1038/s41598-019-45839-z.

Andersson L, Archibald AL, Bottema CD, Brauning R, Burgess SC, Burt DW, Casas E, Cheng HH, Clarke L, Couldrey C et al. 2015. Coordinated international action to accelerate genome-to-phenome with FAANG, the Functional Annotation of Animal Genomes project. *Genome Biology*, **16**(1), 57. doi: 10.1186/s13059-015-0622-4.

Andrews S. 2010. FastQC: A Quality Control Tool for High Throughput Sequence Data. Available online at: http://www.bioinformatics.babraham.ac.uk/projects/fastqc/

APROMAR. 2022. La acuicultura en España 2022. *Asociación Empresarial de Acuicultura de España, Cádiz* (Online, accessed October 17, 2023 at www.apromar.es)

Aramburu O, Blanco A, Bouza C, Martínez P. 2023. Integration of host-pathogen functional genomics data into the chromosome-level genome assembly of turbot (*Scophthalmus maximus*). *Aquaculture*, **564**, 739067. doi: 10.1016/j.aquaculture.2022.739067.

Bangera R, Ødegård J, Præbel AK, Mortensen A, Nielsen HM. 2011. Genetic correlations between growth rate and resistance to vibriosis and viral nervous necrosis in Atlantic cod (*Gadus morhua* L.). *Aquaculture*, **317**(1–4), 67–73. doi: 10.1016/j.aquaculture.2011.04.018.

Baranasic D, Hörtenhuber M, Balwierz PJ, Zehnder T, Mukarram AK, Nepal C, Várnai C, Hadzhiev Y, Jimenez-Gonzalez A, Li N et al. 2022. Multiomic atlas with functional stratification and developmental dynamics of zebrafish cis-regulatory elements. *Nat Genet* **54**, 1037–1050 (2022). doi: 10.1038/s41588-022-01089-w.

Barbieri M, Xie SQ, Torlai-Triglia E, Chiariello AM, Bianco S, de Santiago I, Branco MR, Rueda D, Nicodemi M, Pombo A. 2017. Active and poised promoter states drive folding of the extended

755 HoxB locus in mouse embryonic stem cells. *Nature Structural & Molecular Biology*, **24**(6), 515–
756 524. doi: 10.1038/nsmb.3402

757 Barman TK, Metzger DW. 2021. Disease Tolerance during Viral-Bacterial Co-Infections. *Viruses*,
758 **13**(12), 2362. doi: 10.3390/v13122362.

759 Barnett DW, Garrison EK, Quinlan AR, Strömberg MP, Marth GT. 2011. BamTools: a C++ API and
760 toolkit for analyzing and managing BAM files. *Bioinformatics*, **27**(12), 1691–1692. doi:
761 10.1093/bioinformatics/btr174.

762 Blumer T, Coto-Llerena M, Duong FHT, Heim MH. 2017. SOCS1 is an inducible negative regulator
763 of interferon λ (IFN-λ)–induced gene expression in vivo. *Journal of Biological Chemistry*, **292**(43),
764 17928–17938. doi: 10.1074/jbc.M117.788877.

765 Boltsis I, Grosveld F, Giraud G, Kolovos P. 2021. Chromatin Conformation in Development and
766 Disease. *Frontiers in Cell and Developmental Biology*, **9**. doi: 10.3389/fcell.2021.723859.

767 Buenrostro JD, Wu B, Chang HY, Greenleaf WJ. 2015. ATAC-seq: A Method for Assaying Chromatin
768 Accessibility Genome-Wide. *Current Protocols in Molecular Biology*, **109**(1). doi:
769 10.1002/0471142727.mb2129s109.

770 Cabrera-Ortega AA, Feinberg D, Liang Y, Rossa C, Graves DT. 2017. The Role of Forkhead Box 1
771 (FOXO1) in the Immune System: Dendritic Cells, T Cells, B Cells, and Hematopoietic Stem Cells.
772 *Critical Reviews in Immunology*, **37**(1), 1–13. doi: 10.1615/CritRevImmunol.2017019636.

773 Chen S, Yang J, Wei Y, Wei X. 2020. Epigenetic regulation of macrophages: from homeostasis
774 maintenance to host defense. *Cellular & Molecular Immunology*, **17**(1), 36–49. doi:
775 10.1038/s41423-019-0315-0.

776 Chen W, Huang J, Wang W, Wang Y, Chen H, Wang Q, Zhang Y, Liu Q, Yang D. 2022. Multi-tissue
777 scRNA-seq reveals immune cell landscape of turbot (*Scophthalmus maximus*). *Fundamental*
778 *Research*, **2**(4), 550–561. doi: 10.1016/j.fmre.2021.12.015.

779 Clark EL, Archibald AL, Daetwyler HD, Groenen MAM, Harrison PW, Houston RD, Kühn C, Lien S,
780 Macqueen DJ, Reecy JM et al. 2020. From FAANG to fork: application of highly annotated
781 genomes to improve farmed animal production. *Genome Biology*, **21**(1), 285. doi:
782 10.1186/s13059-020-02197-8.

783 Clark TC, Boudinot P, Collet B. 2021. Evolution of the IRF Family in Salmonids. *Genes*, **12**(2), 238.
784 doi: 10.3390/genes12020238.

785 Clark TC, Naseer S, Gundappa MK, Laurent A, Perquis A, Collet B, Macqueen DJ, Martin SAM,
786 Boudinot P. 2023. Conserved and divergent arms of the antiviral response in the duplicated
787 genomes of salmonid fishes. *Genomics*, **115**(4), 110663. doi: 10.1016/j.ygeno.2023.110663.

788 Corces MR, Trevino AE, Hamilton EG, Greenside PG, Sinnott-Armstrong NA, Vesuna S, Satpathy
789 AT, Rubin AJ, Montine KS, Wu B et al. 2017. An improved ATAC-seq protocol reduces background
790 and enables interrogation of frozen tissues. *Nature Methods*, **14**(10), 959–962. doi:
791 10.1038/nmeth.4396.

792 Cuvier O, Fierz B. 2017. Dynamic chromatin technologies: from individual molecules to
793 epigenomic regulation in cells. *Nature Reviews Genetics*, **18**(8), 457–472. doi:
794 10.1038/nrg.2017.28.

Danecek P, Bonfield JK, Liddle J, Marshall J, Ohan V, Pollard MO, Whitwham A, Keane T, McCarthy SA, Davies RM et al. 2021. Twelve years of SAMtools and BCFtools. *GigaScience*, **10**(2). doi: 10.1093/gigascience/giab008

Díaz-Rosales P, Romero A, Balseiro P, Dios S, Novoa B, Figueras A. 2012. Microarray-Based Identification of Differentially Expressed Genes in Families of Turbot (*Scophthalmus maximus*) After Infection with Viral Haemorrhagic Septicaemia Virus (VHSV). *Marine Biotechnology*, **14**(5), 515–529. doi:10.1007/s10126-012-9465-0.

Dobin A, Davis CA, Schlesinger F, Drenkow J, Zaleski C, Jha S, Batut P, Chaisson M, Gingeras TR. 2013. STAR: ultrafast universal RNA-seq aligner. *Bioinformatics*, **29**(1), 15–21. doi: 10.1093/bioinformatics/bts635.

Domínguez B, Pardo BG, Noia M, Millán A, Gómez-Tato A, Martínez P, Leiro J, Lamas J. 2013. Microarray analysis of the inflammatory and immune responses in head kidney turbot leucocytes treated with resveratrol. *International Immunopharmacology*, **15**(3), 588–596. doi: 10.1016/j.intimp.2013.01.024.

Ecker S, Pancaldi V, Valencia A, Beck S, Paul DS. 2018. Epigenetic and Transcriptional Variability Shape Phenotypic Plasticity. *BioEssays*, **40**(2), 1700148. doi: 10.1002/bies.201700148.

Ernst J, Kellis M. 2012. ChromHMM: automating chromatin-state discovery and characterization. *Nature Methods*, **9**(3), 215–216. doi: 10.1038/nmeth.1906.

Ewels P, Peltzer A, Fillinger S, Patel H, Alneberg J, Wilm A, Ulysse-Garcia M, Di Tommaso P, Nahnsen S. 2023. The nf-core framework for community-curated bioinformatics pipelines. *Zenodo*. doi: 10.5281/zenodo.3240506.

Fang L, Liu S, Liu M, Kang X, Lin S, Li B, Connor EE, Baldwin RL, Tenesa A, Ma L et al. 2019. Functional annotation of the cattle genome through systematic discovery and characterization of chromatin states and butyrate-induced variations. *BMC Biology*, **17**(1), 68. doi: 10.1186/s12915-019-0687-8.

Feinberg AP. 2007. Phenotypic plasticity and the epigenetics of human disease. *Nature*, **447**(7143), 433–440. doi: 10.1038/nature05919.

Figueras A, Robledo D, Corvelo A, Hermida M, Pereiro P, Rubiolo JA, Gómez-Garrido J, Carreté L, Bello X, Gut M et al. 2016. Whole genome sequencing of turbot (*Scophthalmus maximus*; *Pleuronectiformes*): a fish adapted to demersal life. *DNA Research*, **23**(3), 181–192. doi: 10.1093/dnares/dsw007.

Foissac S, Djebali S, Munyard K, Vialaneix N, Rau A, Muret K, Esquerré D, Zytnicki M, Derrien T, Bardou P et al. 2019. Multi-species annotation of transcriptome and chromatin structure in domesticated animals. *BMC Biology*, **17**(1), 108. doi: 10.1186/s12915-019-0726-5.

Frankish A, Carbonell-Sala S, Diekhans M, Jungreis I, Loveland JE, Mudge JM, Sisu C, Wright JC, Arnan C, Barnes I et al. 2023. GENCODE: reference annotation for the human and mouse genomes in 2023. *Nucleic Acids Research*, **51**(D1), D942–D949. doi: 10.1093/nar/gkac1071

Fraslin C, Quillet E, Rochat T, Dechamp N, Bernardet JF, Collet B, Lallias D, Boudinot P. 2020. Combining Multiple Approaches and Models to Dissect the Genetic Architecture of Resistance to Infections in Fish. *Frontiers in Genetics*, **11**. doi: 10.3389/fgene.2020.00677.

835 Gan Z, Chen SN, Huang B, Zou J, Nie P. 2020. Fish type I and type II interferons: composition,
836 receptor usage, production and function. *Reviews in Aquaculture*, **12**(2), 773–804. doi:
837 10.1111/raq.12349.

838 Gao Y, Wang Q, Liu Y, Ma Y, Jin H, Liu J, Wang H, Yan Y, Li J. 2023. Epidemiology of turbot bacterial
839 diseases in China between October 2016 and December 2019. *Frontiers in Marine Science*, **10**.
840 doi: 10.3389/fmars.2023.1145083.

841 Ge SX, Jung D, Yao R. 2020. ShinyGO: a graphical gene-set enrichment tool for animals and
842 plants. *Bioinformatics*, **36**(8), 2628–2629. doi: 10.1093/bioinformatics/btz931.

843 Graves DT, Milovanova TN. 2019. Mucosal Immunity and the FOXO1 Transcription Factors.
844 *Frontiers in Immunology*, **10**. doi: 10.3389/fimmu.2019.02530.

845 Guerrero-Peña L, Suarez-Bregua P, Gil-Gálvez A, Naranjo S, Méndez-Martínez L, Tur R, García-
846 Fernández P, Tena JJ, Rotllant J. 2023. Genome-wide chromatin accessibility and gene expression
847 profiling during flatfish metamorphosis. *Scientific Data*, **10**(1), 196. doi: 10.1038/s41597-023-
848 02111-4.

849 Geven EJW, Klaren PHM. 2017. The teleost head kidney: Integrating thyroid and immune
850 signalling. *Developmental & Comparative Immunology*, 66, 73–83. doi:
851 10.1016/j.dci.2016.06.025.

852 Giral H, Landmesser U, Kratzer A. 2018. Into the Wild: GWAS Exploration of Non-coding RNAs.
853 *Frontiers in Cardiovascular Medicine*, **5**. doi: 10.3389/fcvm.2018.00181.

854 Giuffra E, Tuggle CK. 2019. Functional Annotation of Animal Genomes (FAANG): Current
855 Achievements and Roadmap. *Annual Review of Animal Biosciences*, **7**(1), 65–88. doi:
856 10.1146/annurev-animal-020518-114913.

857 Halstead MM, Ma X, Zhou C, Schultz RM, Ross PJ. 2020. Chromatin remodelling in bovine
858 embryos indicates species-specific regulation of genome activation. *Nature Communications*,
859 **11**(1), 4654. doi: 10.1038/s41467-020-18508-3.

860 Halstead MM, Islas-Trejo A, Goszczynski DE, Medrano JF, Zhou H, Ross PJ. 2021. Large-Scale
861 Multiplexing Permits Full-Length Transcriptome Annotation of 32 Bovine Tissues from a Single
862 Nanopore Flow Cell. *Frontiers in Genetics*, **12**. doi: 10.3389/fgene.2021.664260.

863 Han C, Huang W, Peng S, Zhou J, Zhan H, Li W, Gong J, Li Q. 2023. Characterization and expression
864 analysis of the interferon regulatory factor (IRF) gene family in zig-zag eel (*Mastacembelus*
865 *armatus*) against *Aeromonas veronii* infection. *Developmental & Comparative Immunology*, **140**,
866 104622. doi: 10.1016/j.dci.2022.104622.

867 Hasanuzzaman AFM, Cao A, Ronza P, Fernández-Boo S, Rubiolo JA, Robledo D, Gómez-Tato A,
868 Alvarez-Dios JA, Pardo BG, Villalba A et al. 2020. New insights into the Manila clam – *Perkinsus*
869 *olseni* interaction based on gene expression analysis of clam hemocytes and parasite
870 trophozoites through in vitro challenges. *International Journal for Parasitology*, **50**(3), 195–208.
871 doi: 10.1016/j.ijpara.2019.11.008.

872 He P, Williams BA, Trout D, Marinov GK, Amrhein H, Berghella L, Goh ST, Plajzer-Frick I, Afzal V,
873 Pennacchio LA et al. 2020. The changing mouse embryo transcriptome at whole tissue and
874 single-cell resolution. *Nature*, **583**(7818), 760–767. doi: 10.1038/s41586-020-2536-x.

875 Heinz S, Benner C, Spann N, Bertolino E, Lin YC, Laslo P, Cheng JX, Murre C, Singh H, Glass CK.
876 2010. Simple Combinations of Lineage-Determining Transcription Factors Prime cis-Regulatory
877 Elements Required for Macrophage and B Cell Identities. *Molecular Cell*, **38**(4), 576–589. doi:
878 10.1016/j.molcel.2010.05.004.

879 Herrera-Uribe J, Liu H, Byrne KA, Bond ZF, Loving CL, Tuggle CK. 2020. Changes in H3K27ac at
880 Gene Regulatory Regions in Porcine Alveolar Macrophages Following LPS or PolyIC Exposure.
881 Frontiers in Genetics, **11**. doi: 10.3389/fgene.2020.00817.

882 Howe FS, Fischl H, Murray SC, Mellor J. 2017. Is H3K4me3 instructive for transcription activation?
883 *BioEssays*, **39**(1), e201600095. doi: 10.1002/bies.201600095.

884 Hu J, Barrett RDH. 2017. Epigenetics in natural animal populations. *Journal of Evolutionary*
885 *Biology*, **30**(9), 1612–1632. doi: 10.1111/jeb.13130.

886 Ippolito GC, Dekker JD, Wang YH, Lee BK, Shaffer AL, Lin J, Wall JK, Lee BS, Staudt LM, Liu YJ et
887 al. 2014. Dendritic cell fate is determined by BCL11A. *Proceedings of the National Academy of*
888 *Sciences*, **111**(11). doi: 10.1073/pnas.1319228111.

889 Ivashkiv LB, Donlin LT. 2014. Regulation of type I interferon responses. *Nature Reviews*
890 *Immunology*, **14**(1), 36–49. doi:10.1038/nri3581.

891 Jo SS and Choi SS. 2019. Analysis of the Functional Relevance of Epigenetic Chromatin Marks in
892 the First Intron Associated with Specific Gene Expression Patterns. *Genome Biology and*
893 *Evolution*, **11**(3), 786–797. doi: 10.1093/gbe/evz033.

894 Johnston AD, Simões-Pires CA, Thompson Tv, Suzuki M, Greally JM. 2019. Functional genetic
895 variants can mediate their regulatory effects through alteration of transcription factor binding.
896 *Nature Communications*, **10**(1), 3472. doi: 10.1038/s41467-019-11412-5.

897 Johnston IA, Kent MP, Boudinot P, Looseley M, Bargelloni L, Faggion S, Merino GA, Ilsley GR,
898 Bobe J, Tsigenopoulos CS et al. 2024. Advancing fish breeding in aquaculture through genome
899 functional annotation. *Aquaculture*, **583**, 740589. doi: 10.1016/j.aquaculture.2024.740589

900 Karimzadeh M, Ernst C, Kundaje A, Hoffman MM. 2018. Umap and Bismap: quantifying genome
901 and methylome mappability. *Nucleic Acids Research*. doi: 10.1093/nar/gky677.

902 Kellis M, Wold B, Snyder MP, Bernstein BE, Kundaje A, Marinov GK, Ward LD, Birney E, Crawford
903 GE, Dekker J et al. 2014. Defining functional DNA elements in the human genome. *Proceedings*
904 *of the National Academy of Sciences*, **111**(17), 6131–6138. doi: 10.1073/pnas.1318948111.

905 Kim J, Lee KW, Lee HJ. 2014. Polyphenols Suppress and Modulate Inflammation. In *Polyphenols*
906 *in Human Health and Disease* (pp. 393–408). Elsevier. doi 10.1016/B978-0-12-398456-2.00029-
907 3.

908 Klosterhoff MC, Pereira-Junio J, Rodrigues RV, Gusmão EP, Sampaio LA, Tesser MB, Romano LA.
909 2015. Ontogenic development of kidney, thymus and spleen and phenotypic expression of CD3
910 and CD4 receptors on the lymphocytes of cobia (*Rachycentroncanadum*). *Anais Da Academia*
911 *Brasileira de Ciências*, **87**(4), 2111–2121. doi: 10.1590/0001-3765201520140623.

912 Kopitar-Jerala N. 2017. The Role of Interferons in Inflammation and Inflammasome Activation.
913 *Frontiers in Immunology*, **8**. doi: 10.3389/fimmu.2017.00873.

Kumar A, Zhang J, Yu FSX. 2006. Toll-like receptor 3 agonist poly(I:C)-induced antiviral response in human corneal epithelial cells. *Immunology*, **117**(1), 11–21. doi: 10.1111/j.1365-2567.2005.02258.x.

Lawson ND, Li R, Shin M, Grosse A, Yukselen O, Stone OA, Kucukural A, Zhu L. 2020. An improved zebrafish transcriptome annotation for sensitive and comprehensive detection of cell type-specific genes. *ELife*, **9**. doi: 10.7554/eLife.55792.

Levraud JP, Jouneau L, Briolat V, Laghi V, Boudinot P. 2019. IFN-Stimulated Genes in Zebrafish and Humans Define an Ancient Arsenal of Antiviral Immunity. *The Journal of Immunology*, **203**(12), 3361–3373. doi: 10.4049/jimmunol.1900804.

Lesch BJ, Page DC. 2014. Poised chromatin in the mammalian germ line. *Development*, **141**(19), 3619–3626. doi: 10.1242/dev.113027.

Li H, Durbin R. 2009. Fast and accurate short read alignment with Burrows–Wheeler transform. *Bioinformatics*, **25**(14), 1754–1760. doi: 10.1093/bioinformatics/btp324.

Li B, Dewey CN. 2011. RSEM: accurate transcript quantification from RNA-Seq data with or without a reference genome. *BMC Bioinformatics*, **12**(1), 323. doi: 10.1186/1471-2105-12-323.

Librán-Pérez M, Pereiro P, Figueras A, Novoa B. 2022. Transcriptome Analysis of Turbot (*Scophthalmus maximus*) Infected With *Aeromonas salmonicida* Reveals a Direct Effect on Leptin Synthesis as a Neuroendocrine Mediator of Inflammation and Metabolism Regulation. *Frontiers in Marine Science*, **9**. doi: 10.3389/fmars.2022.888115.

Liu S, Yu Y, Zhang S, Cole JB, Tenesa A, Wang T, McDaneld TG, Ma L, Liu GE, Fang L. 2020. Epigenomics and genotype-phenotype association analyses reveal conserved genetic architecture of complex traits in cattle and human. *BMC Biology*, **18**(1), 80. doi: 10.1186/s12915-020-00792-6.

Love MI, Huber W, Anders S. 2014. Moderated estimation of fold change and dispersion for RNA-seq data with DESeq2. *Genome Biology*, **15**(12), 550. doi: 10.1186/s13059-014-0550-8.

Marinis JM, Hutti JE, Homer CR, Cobb BA, Cantley LC, McDonald C, Abbott DW. 2012. IκB Kinase *α* Phosphorylation of TRAF4 Downregulates Innate Immune Signaling. *Molecular and Cellular Biology*, **32**(13), 2479–2489. doi: 10.1128/MCB.00106-12.

Maroso F, Hermida M, Millán A, Blanco A, Saura M, Fernández A, Dalla-Rovere G, Bargelloni L, Cabaleiro S, Villanueva B et al. 2018. Highly dense linkage maps from 31 full-sibling families of turbot (*Scophthalmus maximus*) provide insights into recombination patterns and chromosome rearrangements throughout a newly refined genome assembly. *DNA Research*, **25**(4), 439–450. doi: 10.1093/dnares/dsy015.

Martin M. 2011. Cutadapt removes adapter sequences from high-throughput sequencing reads. *EMBnet.Journal*, **17**(1), 10. doi: 10.14806/ej.17.1.200

Martínez P. 2016. Genomics advances for boosting aquaculture breeding programs in Spain. *Aquaculture*, **464**, 117–120. doi: 10.1016/j.aquaculture.2016.06.021.

Martínez P, Robledo D, Taboada X, Blanco A, Moser M, Maroso F, Hermida M, Gómez-Tato A, Álvarez-Blázquez B, Cabaleiro S et al. 2021. A genome-wide association study, supported by a

new chromosome-level genome assembly, suggests sox2 as a main driver of the undifferentiatiated ZZ/ZW sex determination of turbot (*Scophthalmus maximus*). *Genomics*, **113**(4), 1705–1718. doi: 10.1016/j.ygeno.2021.04.007.

Martínez de Paz A, Josefowicz SZ. 2021. Signaling-to-chromatin pathways in the immune system. *Immunological Reviews*, **300**(1), 37–53. doi: 10.1111/imr.12955.

Millán A, Gómez-Tato A, Fernández C, Pardo BG, Álvarez-Dios JA, Calaza M, Bouza C, Vázquez M, Cabaleiro S, Martínez P. 2010. Design and Performance of a Turbot (*Scophthalmus maximus*) Oligo-microarray Based on ESTs from Immune Tissues. *Marine Biotechnology*, **12**(4), 452–465. doi: 10.1007/s10126-009-9231-0.

Millán A, Gómez-Tato A, Pardo BG, Fernández C, Bouza C, Vera M, Alvarez-Dios JA, Cabaleiro S, Lamas J, Lemos ML et al. 2011. Gene Expression Profiles of the Spleen, Liver, and Head Kidney in Turbot (*Scophthalmus maximus*) Along the Infection Process with *Aeromonas salmonicida* Using an Immune-Enriched Oligo-microarray. *Marine Biotechnology*, **13**(6), 1099–1114. doi: 10.1007/s10126-011-9374-7.

Mishra S, Das R, Swain P. 2018. Status of Fish Diseases in Aquaculture and Assessment of Economic Loss Due to Disease; Today and Tomorrow's Printers and Publishers: New Delhi, India, Volume 1.

Moazed D. 2011. Mechanisms for the Inheritance of Chromatin States. *Cell*, **146**(4), 510–518. doi: 10.1016/j.cell.2011.07.013.

Mokhtar DM, Zaccone G, Alesci A, Kuciel M, Hussein MT, Sayed RKA. 2023. Main Components of Fish Immunity: An Overview of the Fish Immune System. *Fishes*, **8**(2), 93. doi: 10.3390/fishes8020093.

Murira A, Lamarre A. 2016. Type-I Interferon Responses: From Friend to Foe in the Battle against Chronic Viral Infection. *Frontiers in Immunology*, **7.** doi: 10.3389/fimmu.2016.00609.

Navarini AA, Recher M, Lang KS, Georgiev P, Meury S, Bergthaler A, Flatz L, Bille J, Landmann R, Odermatt B et al. 2006. Increased susceptibility to bacterial superinfection as a consequence of innate antiviral responses. *Proceedings of the National Academy of Sciences*, **103**(42), 15535–15539. doi: 10.1073/pnas.0607325103.

Nie L, Xu XX, Xiang LX, Shao JZ, Chen J. 2017. Mutual Regulation of NOD2 and RIG-I in Zebrafish Provides Insights into the Coordination between Innate Antibacterial and Antiviral Signaling Pathways. *International Journal of Molecular Sciences*, **18**(6), 1147. doi: 10.3390/ijms18061147.

Ødegård J, Olesen I, Gjerde B, Klemetsdal G. 2007. Positive genetic correlation between resistance to bacterial (furunculosis) and viral (infectious salmon anaemia) diseases in farmed Atlantic salmon (*Salmo salar*). *Aquaculture,* ***271***(1–4), 173–177. doi: 10.1016/j.aquaculture.2007.06.006.

Ødegård J, Baranski M, Gjerde B, Gjedrem T. 2011. Methodology for genetic evaluation of disease resistance in aquaculture species: challenges and future prospects. *Aquaculture Research*, **42**, 103–114. doi: 10.1111/j.1365-2109.2010.02669.x.

Overbey EG, Ng TT, Catini P, Griggs LM, StewartP, Tkalcic S, Hawkins RD, Drechsler Y. 2021. Transcriptomes of an Array of Chbiicken Ovary, Intestinal, and Immune Cells and Tissues. *Frontiers in Genetics*, **12**. doi: 10.3389/fgene.2021.664424.

Pan Z, Yao Y, Yin H, Cai Z, Wang Y, Bai L, Kern C, Halstead M, Chanthavixay G, Trakooljul N et al. 2021. Pig genome functional annotation enhances the biological interpretation of complex traits and human disease. *Nature Communications*, **12**(1), 5848. doi: 10.1038/s41467-021-26153-7.

Pan Z, Wang Y, Wang M, Wang Y, Zhu X, Gu S, Zhong C, An L, Shan M, Damas J et al. 2023. An atlas of regulatory elements in chicken: A resource for chicken genetics and genomics. *Science Advances*, **9**(18). doi: 10.1126/sciadv.ade1204.

Pardo BG, Fernández C, Millán A, Bouza C, Vázquez-López A, Vera M, Alvarez-Dios JA, Calaza M, Gómez-Tato A, Vázquez M et al. 2008. Expressed sequence tags (ESTs) from immune tissues of turbot (*Scophthalmus maximus*) challenged with pathogens. *BMC Veterinary Research*, **4**(1), 37. doi: 10.1186/1746-6148-4-37.

Pardo BG, Millán A, Gómez-Tato A, Fernández C, Bouza C, Alvarez-Dios JA, Cabaleiro S, Lamas J, Leiro JM, Martínez P. 2012. Gene Expression Profiles of Spleen, Liver, and Head Kidney in Turbot (*Scophthalmus maximus*) Along the Infection Process with *Philasterides dicentrarchi* Using an Immune-Enriched Oligo-Microarray. *Marine Biotechnology*, **14**(5), 570–582. doi: 10.1007/s10126-012-9440-9.

Park PJ. 2009. ChIP–seq: advantages and challenges of a maturing technology. *Nature Reviews Genetics*, **10**(10), 669–680. doi: 10.1038/nrg2641.

Patel H, Ewels P, Peltzer A, Botvinnik O, Sturm G, Moreno D, Vemuri P, Garcia MU, Morins S, Pantano L et al. 2023. nf-core/rnaseq: nf-core/rnaseq v3.10.1 – Plastered Rhodium Rudolph. *Zenodo*. doi: 10.5281/zenodo.7505987.

Prowse-Wilkins CP, Wang J, Xiang R, Garner JB, Goddard ME, Chamberlain AJ. 2021. Putative Causal Variants Are Enriched in Annotated Functional Regions From Six Bovine Tissues. *Frontiers in Genetics*, **12**. doi: 10.3389/fgene.2021.664379.

Raghavan V, Kraft L, Mesny F, Rigerte L. 2022. A simple guide to *de novo* transcriptome assembly and annotation. *Briefings in Bioinformatics*, **23**(2). doi: 10.1093/bib/bbab563.

Ramberg S, Høyheim B, Østbye TKK, Andreassen R. 2021. A *de novo* Full-Length mRNA Transcriptome Generated from Hybrid-Corrected PacBio Long-Reads Improves the Transcript Annotation and Identifies Thousands of Novel Splice Variants in Atlantic Salmon. *Frontiers in Genetics*, **12**. doi: 10.3389/fgene.2021.656334.

Ramírez F, Dündar F, Diehl S, Grüning BA, Manke T. 2014. deepTools: a flexible platform for exploring deep-sequencing data. *Nucleic Acids Research*, **42**(W1), W187–W191. doi: 10.1093/nar/gku365.

Robinson JT, Thorvaldsdottir H, Turner D, Mesirov JP. 2023. igv.js: an embeddable JavaScript implementation of the Integrative Genomics Viewer (IGV). *Bioinformatics*, **39**(1). doi: 10.1093/bioinformatics/btac830.

1030 Robledo D, Ronza P, Harrison PW, Losada AP, Bermúdez R, Pardo BG, José-Redondo M, Sitjà-
1031 Bobadilla A, Quiroga MI, Martínez P. 2014. RNA-seq analysis reveals significant transcriptome
1032 changes in turbot (*Scophthalmus maximus*) suffering severe enteromyxosis. *BMC Genomics*,
1033 **15**(1), 1149. doi: 10.1186/1471-2164-15-1149.

1034 Robledo D, Martin AP, Álvarez-Dios JA, Bouza C, Pardo BG, Martínez P. 2017. First characterization
1035 and validation of turbot microRNAs. *Aquaculture*, **472**, 76–83. doi:
1036 10.1016/j.aquaculture.2016.05.002.

1037 Ronza P, Robledo D, Bermúdez R, Losada AP, Pardo BG, Sitjà-Bobadilla A, Quiroga MI, Martínez P.
1038 2016. RNA-seq analysis of early enteromyxosis in turbot (*Scophthalmus maximus*): new insights
1039 into parasite invasion and immune evasion strategies. *International Journal for Parasitology*,
1040 **46**(8), 507–517. doi: 10.1016/j.ijpara.2016.03.007.

1041 Ronza P, Robledo D, Losada AP, Bermúdez R, Pardo BG, Martínez P, Quiroga MI. 2020. The
1042 Teleost Thymus in Health and Disease: New Insights from Transcriptomic and Histopathological
1043 Analyses of Turbot, *Scophthalmus maximus*. *Biology*, **9**(8), 221. doi: 10.3390/biology9080221.

1044 Saeed S, Quintin J, Kerstens HHD, Rao NA, Aghajanirefah A, Matarese F, Cheng SC, Ratter J,
1045 Berentsen K, van der Ent MA et al. 2011. Role of the Inflammasome, IL-1β, and IL-18 in Bacterial
1046 Infections. *The Scientific World JOURNAL*, **11**, 2037–2050. doi: 10.1100/2011/212680.

1047 Saura M, Carabaño MJ, Fernández A, Cabaleiro S, Doeschl-Wilson AB, Anacleto O, Maroso F,
1048 Millán A, Hermida M, Fernández C et al. 2019. Disentangling Genetic Variation for Resistance
1049 and Endurance to Scuticociliatosis in Turbot Using Pedigree and Genomic Information. *Frontiers*
1050 *in Genetics*, **10**. doi: 10.3389/fgene.2019.00539.

1051 Secombes CJ, Wang T, Hong S, Peddie S, Crampe M, Laing KJ, Cunningham C, Zou J. 2001.
1052 Cytokines and innate immunity of fish. *Developmental & Comparative Immunology*, **25**(8–9),
1053 713–723. doi: 10.1016/S0145-305X(01)00032-5.

1054 Shan S, Liu R, Jiang L, Zhu Y, Li H, Xing W, Yang G. 2018. Carp Toll-like receptor 8 (Tlr8): An
1055 intracellular Tlr that recruits TIRAP as adaptor and activates AP-1 pathway in immune response.
1056 *Fish & Shellfish Immunology*, *82*, 41–49. doi: 10.1016/j.fsi.2018.08.001.

1057 Stark R, Brown G. 2011. DiffBind: differential binding analysis of ChIP-Seq peak data.
1058 *Bioconductor*. doi: 10.18129/B9.bioc.DiffBind.

1059 Stępniak K, Machnicka MA, Mieczkowski J, Macioszek A, Wojtaś B, Gielniewski B, Poleszak K,
1060 Perycz M, Król SK, Guzik R et al. 2021. Mapping chromatin accessibility and active regulatory
1061 elements reveals pathological mechanisms in human gliomas. *Nature Communications*, **12**(1),
1062 3621. doi: 10.1038/s41467-021-23922-2.

1063 Srour N, Khan S, Richard S. 2022. The Influence of Arginine Methylation in Immunity and
1064 Inflammation. *Journal of Inflammation Research*, *Volume* **15**, 2939–2958. doi:
1065 10.2147/JIR.S364190.

1066 Subasinghe R, Soto D, Jia J. 2009. Global aquaculture and its role in sustainable development.
1067 *Reviews in Aquaculture*, **1**(1), 2–9. doi: 10.1111/j.1753-5131.2008.01002.x.

Sullivan C, Soos BL, Millard PJ, Kim CH, King BL. 2021. Modeling Virus-Induced Inflammation in Zebrafish: A Balance Between Infection Control and Excessive Inflammation. *Frontiers in Immunology*, **12**. doi: 10.3389/fimmu.2021.636623.

Summers KM, Bush SJ, Wu C, Su AI, Muriuki C, Clark EL, Finlayson HA, Eory L, Waddell LA, Talbot R et al. 2020. Functional Annotation of the Transcriptome of the Pig, *Sus scrofa*, Based Upon Network Analysis of an RNAseq Transcriptional Atlas. *Frontiers in Genetics*, **10**. doi: 10.3389/fgene.2019.01355.

Sun K, Metzger DW. 2008. Inhibition of pulmonary antibacterial defense by interferon-γ during recovery from influenza infection. *Nature Medicine*, **14**(5), 558–564. doi: 10.1038/nm1765.

Taylor RS, Ruiz Daniels R, Dobie R, Naseer S, Clark TC, Henderson NC, Boudinot P, Martin SAM, Macqueen DJ. 2022. Single cell transcriptomics of Atlantic salmon (*Salmo salar* L.) liver reveals cellular heterogeneity and immunological responses to challenge by Aeromonas salmonicida. *Frontiers in Immunology*, **13**. doi: 10.3389/fimmu.2022.984799.

Troell M, Costa-Pierce B, Stead S, Cottrell RS, Brugere C, Farmery AK, Little DC, Strand Å, Pullin R, Soto D et al. 2023. Perspectives on aquaculture's contribution to the Sustainable Development Goals for improved human and planetary health. *Journal of the World Aquaculture Society*, **54**(2), 251–342. doi: 10.1111/jwas.12946.

Tuggle CK, Giuffra E, White SN, Clarke L, Zhou H, Ross PJ, Acloque H, Reecy JM, Archibald A, Bellone RR et al. 2016. GO-FAANG meeting: a Gathering On Functional Annotation of Animal Genomes. *Animal Genetics*, **47**(5), 528–533. doi: 10.1111/age.12466.

Turkistany SA, DeKoter RP. 2011. The Transcription Factor PU.1 is a Critical Regulator of Cellular Communication in the Immune System. *Archivum Immunologiae et Therapiae Experimentalis*, **59**(6), 431–440. doi: 10.1007/s00005-011-0147-9.

Valle A, Leiro JM, Pereiro P, Figueras A, Novoa B, Dirks RPH, Lamas J. 2020. Interactions between the Parasite Philasterides dicentrarchi and the Immune System of the Turbot *Scophthalmus maximus*. A Transcriptomic Analysis. *Biology*, **9**(10), 337. doi: 10.3390/biology9100337

van Berkum NL, Lieberman-Aiden E, Williams L, Imakaev M, Gnirke A, Mirny LA, Dekker J, Lander ES. 2010. Hi-C: A Method to Study the Three-dimensional Architecture of Genomes. *Journal of Visualized Experiments*, **39**. doi: 10.3791/1869.

Villar D, Frost S, Deloukas P, Tinker A. 2020. The contribution of non-coding regulatory elements to cardiovascular disease. *Open Biology*, **10**(7). doi: 10.1098/rsob.200088.

Vu H, Ernst J. 2022. Universal annotation of the human genome through integration of over a thousand epigenomic datasets. *Genome Biology*, **23**(1), 9. doi: 10.1186/s13059-021-02572-z.

Watson DK, Li R, Sementchenko VI, Mavrothalassitis G, Seth A. 2002. ETS Family of Transcription Factors. In *Encyclopedia of Cancer* (pp. 189–196). Elsevier. doi: 10.1016/B0-12-227555-1/00078-2.

Weidemüller P, Kholmatov M, Petsalaki E, Zaugg JB. 2021.. Transcription factors: Bridge between cell signaling and gene regulation. *PROTEOMICS*, **21**(23–24). doi: 10.1002/pmic.202000034.

Xiang R, MacLeod IM, Daetwyler HD, de Jong G, O'Connor E, Schrooten C, Chamberlain AJ, Goddard ME. 2021. Genome-wide fine-mapping identifies pleiotropic and functional variants

that predict many traits across global cattle populations. *Nature Communications*, **12**(1), 860. doi: 10.1038/s41467-021-21001-0.

Xu X, Shao C, Xu H, Zhou Q, You F, Wang N, Li W, Li M, Chen S. 2020. Draft genomes of female and male turbot *Scophthalmus maximus*. *Scientific Data*, **7**(1), 90. doi: 10.1038/s41597-020-0426-6.

Yan F, Powell DR, Curtis DJ, Wong NC. 2020a. From reads to insight: a hitchhiker's guide to ATAC-seq data analysis. *Genome Biology*, **21**(1), 22. doi: 10.1186/s13059-020-1929-3.

Yan X, Zhao X, Huo R, Xu T. 2020b. IRF3 and IRF8 Regulate NF-κB Signaling by Targeting MyD88 in Teleost Fish. *Frontiers in Immunology*, **11**. doi: 10.3389/fimmu.2020.00606.

Yu Y, Wang J, Khaled W, Burke S, Li P, Chen X, Yang W, Jenkins NA, Copeland NG, Zhang S et al. 2012. Bcl11a is essential for lymphoid development and negatively regulates p53. *Journal of Experimental Medicine*, **209**(13), 2467–2483. doi: 10.1084/jem.20121846.

Zhang Y, Liu T, Meyer CA, Eeckhoute J, Johnson DS, Bernstein BE, Nusbaum C, Myers RM, Brown M, Li W et al. 2008. Model-based Analysis of ChIP-Seq (MACS). *Genome Biology*, **9**(9), R137. doi: 10.1186/gb-2008-9-9-r137.

Zhang R, Kang R, Tang D. 2021. The STING1 network regulates autophagy and cell death. *Signal Transduction and Targeted Therapy*, **6**(1), 208. doi: 10.1038/s41392-021-00613-4.

Zhou Y, Zhou B, Pache L, Chang M, Khodabakhshi AH, Tanaseichuk O, Benner C, Chanda SK. 2019. Metascape provides a biologist-oriented resource for the analysis of systems-level datasets. *Nature Communications*, **10**(1), 1523. doi: 10.1038/s41467-019-09234-6.

Zhu M, John S, Berg M, Leonard WJ. 1999. Functional Association of Nmi with Stat5 and Stat1 in IL-2- and IFN γ-Mediated Signaling. *Cell*, **96**(1), 121–130. doi: 10.1016/S0092-8674(00)80965-4.

Zhu XN, Wang YZ, Li C, Wu HY, Zhang R, Hu XX. 2023. Chicken chromatin accessibility atlas accelerates epigenetic annotation of birds and gene fine-mapping associated with growth traits. *Zoological Research*, **44**(1), 53–62. doi: 10.24272/j.issn.2095-8137.2022.228.